

Propagation of Interplanetary Shocks in the Heliosphere

M. Lkhagvadorj^{1,2}, G. Facskó^{1,3,4,5}, A. Opitz¹, P. Kovács¹, D. G. Sibeck⁴

¹Department of Space Physics and Space Technology, Wigner Research Centre for Physics

²Faculty of Science, Eötvös Loránd University

³Department of Informatics, Milton Friedman University

⁴NASA Goddard Space Flight Center

⁵the Catholic University of America

¹Konkoly-Thege Miklós út 29-33., H-1121 Budapest, Hungary

²Pázmány Péter sétány 1/A, H-1117 Budapest, Hungary

³H-1039 Budapest, Kelta utca 2., Budapest, Hungary

⁴48800 Greenbelt Rd, Greenbelt, MD 20771, USA

⁵620 Michigan Ave NE, Washington, DC 20064, USA

Key Points:

- Wave dispersion of IP shocks cannot be observed in the range of 40 million km.
- The shape of two IP shocks is determined from conjugated spacecraft observations.
- These IP shocks are developed from coronal interaction regions.

18 **Abstract**

19 Interplanetary shocks are one of the crucial dynamic processes in the Heliosphere. They
 20 accelerate particles into a high energy, generate plasma waves, and could potentially trig-
 21 ger geomagnetic storms in the terrestrial magnetosphere disturbing significantly our tech-
 22 nological infrastructures. In this study, two IP shock events are selected to study the tem-
 23 poral variations of the shock parameters using magnetometer and ion plasma measure-
 24 ments of the STEREO–A and B, the Wind, Cluster fleet, and the ACE spacecraft. The
 25 shock normal vectors are determined using the minimum variance analysis (MVA) and
 26 the magnetic coplanarity methods (CP). During the May 7 event, the shock parameters
 27 and the shock normal direction are consistent. The shock surface appears to be tilted
 28 almost the same degree as the Parker spiral, and the driver could be a CIR. During the
 29 April 23 event, the shock parameters do not change significantly except for the shock θ_{Bn}
 30 angle, however, the shape of the IP shock appears to be twisted along the transverse di-
 31 rection to the Sun-Earth line as well. The driver of this rippled shock is SIRs/CIRs as
 32 well. Being a fast-reverse shock caused this irregularity in shape.

33 **Plain Language Summary**

34 The Sun dominates the Solar System gravitationally, magnetically, and by a very
 35 fast magnetized flow, called solar wind. In this matter strong and steep waves are mov-
 36 ing, so-called interplanetary (IP) shocks. The parameters of the solar wind, the density,
 37 the magnetic field, the solar wind speed, and the temperature jump when you pass these
 38 waves. These IP shocks are usually measured by a single spacecraft. Therefore, their shape
 39 is supposed to be a plane. Using various multiple probes we determine the shape of two
 40 IP shocks. Additionally, we check whether the parameters of shocks change temporar-
 41 ily. If you throw a stone into a lake circular waves are triggered on the surface of the wa-
 42 ter. During their propagation, the width of the wave increases because the waves are a
 43 branch of waves, the so-called wave package. The wave package consists of waves prop-
 44 agating at different speeds. This feature is called wave dispersion. You cannot see any
 45 sign of wave dispersion or temporal development of the IP shock in the range of 40 million km.

46 **1 Introduction**

47 The solar corona is hotter than the photosphere, the chromosphere, and the tran-
 48 sient layers beneath it. As a result, the high temperatures ionize atoms, creating a plasma
 49 of free-moving electrons and ions, the so-called the solar wind. Historically, (Parker, 1958)
 50 predicted the existence of the solar wind and made the term. He deducted it based on
 51 German astronomer Ludwig Bierman's observation of how the comet tail always points
 52 away from the Sun (Biermann, 1957). The existence of the solar wind was confirmed by
 53 the Mariner 2 spacecraft (Snyder & Neugebauer, 1965). The solar wind is a collisionless
 54 plasma, and it flows at both supersonic and super-Alfvénic speed, meaning they exceed
 55 the Alfvén speed, which is the speed of magnetohydrodynamic waves in a plasma. A shock
 56 wave is where a fluid changes from supersonic to subsonic speed. Therefore, the fast-moving
 57 solar wind tends to create a shock on its journey. Hence, interplanetary (IP) shocks are
 58 common through the heliosphere, which is a bubble-like region of space surrounding the
 59 Sun and extending far beyond the orbits of the planets and is filled with the solar wind.
 60 There are a few varieties of shocks such as planetary bow shocks, shocks that are risen
 61 due to the stream interaction regions (SIR), which is called co-rotation interaction re-
 62 gion (CIR) when extending beyond 1 AU, and coronal mass ejection (CME) driven shocks.
 63 IP shocks are one of the main and efficient accelerators of energetic particles (Tsurutani
 64 & Lin, 1985; Keith & Heikkila, 2021). These accelerated particles can cause disturbances
 65 to the geomagnetic field and are hazardous to astronauts and satellites. (IP) shocks driven
 66 by CMEs triggers large geomagnetic storms (Gonzalez et al., 1994). Large geomagnetic
 67 storms can damage oil and gas pipelines and interfere with electrical power infrastruc-

tures. GPS navigation and high-frequency radio communications are also affected by ionosphere changes brought on by geomagnetic storms (Cid et al., 2014) and can cause internet disruptions around the world for many months (Jyothi, 2021). Therefore, IP shocks are important in determining and understanding space weather.

The main goal of this paper is to study and determine parameters such as IP shock normals, upstream and downstream plasma parameters (magnetic field, density, temperature, velocity), and how they vary in their temporal evolution. There are several methods for determining the shock normal vector (Schwartz, 1998). Here, the minimum variance analysis (MVA) and the magnetic coplanarity method (CP) are used. These two methods are primarily utilized because they require solely magnetic field data. The data are from NASA Solar Terrestrial Relations Observatory (STEREO; Kaiser et al., 2008), the Wind (Ogilvie et al., 1995), and Advanced Composition Explorer (ACE; Stone et al., 1998), and ESA Cluster fleet (Escoubet et al., 2001). The temporal resolution of the magnetometers of the spacecraft is significantly higher than the plasma instruments because the variations are quite slow in the heliosphere. Hence, any agreement between the two methods indicates relatively accurate shock normal vectors (Facskó et al., 2008, 2009, 2010).

Here, two events are studied, one is on May 7, 2007, and the other is on April 23, 2007. The year 2007, is special because it was the year when the twin STEREO–A and B spacecraft were closer to the Sun-Earth line until their gradual separation from each other in the following years. Later, the spatial separation is so high that it is hard to distinguish the spatial and temporal changes. Hence, shocks during this period are proper to study shock propagation and their temporal developments in the case of using these spacecraft.

2 Missions and instruments

In this paper, STEREO A and B, Wind, ACE, and the Cluster spacecraft magnetic field, ion plasma, and spacecraft potential data are used.

2.1 The STEREO mission

The twin STEREO A and B spacecraft were launched on October 26, 2006, from Kennedy Space Center (Kaiser et al., 2008). In heliospheric orbit at 1 AU, STEREO–A (Ahead) leads while STEREO–B (Behind) trails Earth. The two spacecraft separate at 44° from each other annually. Both spacecraft were equipped with the complement of four scientific instruments, particularly two instruments and two instrument suites, with a total of 13 instruments on each spacecraft.

The PLAsma and SupraThermal Ion Composition (PLASTIC) instrument measures proton, the composition of heavy ions, and alpha particles in the solar wind plasma (Galvin et al., 2008). The In-situ Measurements of Particles and CME Transients magnetic field experiment (IMPACT) suite of instruments consists of seven instruments, and three of them are located on the 6-meter boom as shown while the others are in the main hull of the spacecraft (Acuña et al., 2008). The IMPACT measures protons, heavy ions, and electrons, and the MAG magnetometer sensor in it measure the in situ magnetic fields in a range of $\pm 512 \text{ nT}$ with 0.1 nT accuracy (Kaiser & Adams, 2007).

We downloaded all data from NASA's Coordinated Data Analysis Web (CDAWeb, <https://cdaweb.gsfc.nasa.gov/>). We obtained the STEREO–A and B magnetic field observation and the ion plasma data from the STEREO IMPACT with the time resolution of 100 ms and the STEREO PLASTIC instruments, respectively. The magnetic field and the plasma data of the STEREO–A and B are in the RTN spacecraft coordi-

115 nate system, where R is radially outward from the Sun, T is along the planetary orbital,
 116 and N is northward direction.

117 2.2 The Wind mission

118 NASA's Wind spacecraft was launched on November 1, 1994, (Wilson et al., 2021).
 119 The Wind was initially planned sent to L_1 Lagrange point, however, was delayed to study
 120 the magnetosphere and lunar environment. Following a sequence of orbital adjustments,
 121 the Wind spacecraft was positioned in a Lissajous orbit close to the L_1 Lagrange point
 122 in early 2004 for studying the incoming solar wind (NASA WIND team, 2020).

123 The spacecraft is equipped with the eight instruments, however, we used only the
 124 Magnetic Field Investigation (MFI; Lepping et al., 1995) and the Solar Wind Experi-
 125 ment (SWE; Ogilvie et al., 1995) measurements in this study. The MFI consists of two
 126 magnetometers at the 12-meter boom, its measurement capability is 4 nT, 65536 nT, and
 127 measures vector magnetic field up in a time resolution of 22 or 11 vectors per second for
 128 the calibrated high-resolution data and primary science data is in time resolutions of three
 129 seconds, one minute and one hour (NASA WIND team, 2022). The SWE measures the
 130 solar wind key parameters such as velocity, density, and temperature.

131 From CDAWeb, we got Wind magnetic and plasma data from the MFI instrument
 132 with a time resolution of 3 s and SWE instrument with a time resolution of 1 min, re-
 133 spectively. The magnetic field and the plasma data of the Wind are in the Geocentric
 134 Solar Ecliptic System (GSE) coordinate system, where X-axis is pointing to the Sun from
 135 the Earth, Y-axis is in the ecliptic plane against the planetary motion, and Z-axis is north-
 136 ward direction.

137 2.3 The ACE mission

138 NASA's ACE spacecraft was launched on August 25, 1997, (Stone et al., 1998). The
 139 spacecraft is located at L_1 Lagrangian point as well as the Wind spacecraft. The space-
 140 craft is equipped with nine primary scientific instruments and one engineering instru-
 141 ment. We used in the study the measurements of the Magnetometer (MAG; Smith et
 142 al., 1998), and the Solar Wind Electron, Proton and Alpha Monitor (SWEPAM; McCo-
 143 mas et al., 1998). The MAG consists of twin triaxial flux-gate magnetometers such that
 144 magnetometer sensors have between 3 and 6 vectors s^{-1} resolutions for continuous ob-
 145 servation of the interplanetary magnetic field (Smith et al., 1998).

146 From CDAWeb, we downloaded the ACE magnetic and plasma data from the ACE
 147 MAG with a time resolution of 1 s SWEPAM with the time resolution of 64 s, respec-
 148 tively. The magnetic field and the plasma data are in both the RTN and GSE coordi-
 149 nate systems.

150 2.4 The Cluster fleet

151 ESA's Cluster constellations consist of four satellites, which were launched on 16
 152 July and 9 August 2000 (Escoubet et al., 2001). The Cluster satellites orbit in a tetra-
 153 hedral formation around Earth. The orbits feature perigees close to four Earth radii (R_E)
 154 and apogees approximately $19.6 R_E$ away (Zhang et al., 2010). The four satellites are
 155 each equipped with 11 instruments. We used the data of the Cluster Ion Composition
 156 (CIS; Reme et al., 1997), the Fluxgate Magnetometer (FGM; Balogh et al., 1997), and
 157 the Electric field and waves (EFW; Gustafsson et al., 1997) instruments in this study
 158 .

159 The FGM is composed of two tri-axial fluxgate magnetometers, which are installed
 160 on one of the two 5-meter radial booms. It measures in the dynamic range $\pm 65,536$ nT.
 161 At the highest dynamic level, the resolution is ± 8 nT, and the time resolution is 100 vec-

162 tors per second (Balogh et al., 1997; Organization, 2021). The CIS instrument measures
 163 three-dimensional ion distribution, and it is composed of two distinct sensors: the Com-
 164 position Distribution Function (CODIF) sensor and the Hot Ion Analyzer (HIA) sen-
 165 sor (Reme et al., 1997). The CIS experiment is not operational for Cluster-2 and the HIA
 166 sensor is switched off for Cluster-4 due to a problem with the high voltage of the elec-
 167 trostatic analyzer (CIS team, 2021). Hence, for Cluster-2 and Cluster-4, the EFW in-
 168 strument measurement is useful (Gustafsson et al., 1997).

169 As the spacecraft travels through the plasma environment, it acquires an electric
 170 charge as a result of contact with charged particles. This charging process results in an
 171 electrical potential discrepancy between the spacecraft and the plasma around it, a phe-
 172 nomenon referred to as spacecraft potential. The EFW instrument measures the space-
 173 craft potential and the electron density of the plasma could be calculated using an em-
 174 pirical formula.

$$N_e = 200(V_{sc})^{-1.85}, \quad (1)$$

175 where N_e is the calculated electron density and V_{sc} is the Cluster EFW spacecraft po-
 176 tential (Sandhu et al., 2016; Trotignon et al., 2010, 2011).

177 From CDAWeb, we acquired the magnetic data of Cluster satellites from the Clus-
 178 ter FGM with a time resolution of 4 s for all the four Cluster satellites, ion data from
 179 the Cluster CIS with a time resolution of 4 s for the Cluster SC1 and SC3 satellites, and
 180 the spacecraft potential data from EFW with a time resolution of 4 s for the Cluster SC2
 181 and SC4 satellites where CIS measurements were not available. All the Cluster data were
 182 in the GSE coordinate system.

183 3 IP shock events and transformations

184 IP shock candidates are chosen from the shock lists in the Database of Heliospheric
 185 Shock Waves maintained at the University of Helsinki <http://www.ipshocks.fi/>. For
 186 the event selection we chose the year 2007 because STEREO–A and STEREO–B were
 187 closer to each other as well as to the Sun-Earth line. Therefore, the two events are from
 188 this year, particularly on May 07, 2007, and April 23, 2007. In the first event, May 07
 189 of 2007, the selected spacecraft are STEREO–A, STEREO–B, Wind, and the four Clus-
 190 ter satellites. For the second event, April 23, 2007, the spacecraft are STEREO–A and
 191 B, ACE, and Wind.

192 After choosing the shock candidates and obtaining the data, we transformed the
 193 coordinate system transformation in such a way that all the coordinate systems are changed
 194 to the Heliocentric Earth Ecliptic (HEE) coordinate system, where the X-axis is toward
 195 the Earth from the Sun, Z-axis is northward direction. This system is fixed with respect
 196 to the Sun-Earth line. To transform from the RTN and the GSE coordinate systems to
 197 the HEE coordinate system, we used Transformation de REpères en Physique Spatiale
 198 (TREPS; <http://treps.irap.omp.eu/>) online tool. The TREPS tool, which is devel-
 199 oped by the French Plasma Physics Data Centre (CDPP), the national data center in
 200 France for the solar system plasmas, is based on SPICE (Spacecraft, Planet, Instrument,
 201 C-matrix, and Events) information system kernels created by National Aeronautics and
 202 Space Administration (NASA)/Navigation and Ancillary Information Facility (NAIF)
 203 tool (Génot et al., 2018).

204 4 Analysis methods

205 We use Minimum Variance Analysis (MVA) and magnetic co-planarity (CP) to de-
 206 termine the IP shock normals (B. U. Ö. Sonnerup & Scheible, 1998; Schwartz, 1998). The
 207 coplanarity methods are based on the magnetic coplanarity theorem, which stated that
 208 both sides of the magnetic field vectors on the shock and the shock normal lie in the same
 209 plane. Similarly, the velocity on both sides or, in other words, the velocity jump through

210 the shock also lie in the same plane. The method of magnetic coplanarity is straightforward
 211 to implement and, it only necessitates the use of a magnetic field data (Paschmann
 212 & Daly, 1998).

213 By comparing the two methods, the upstream and downstream time intervals of
 214 the magnetic field measurements are set. We set up the following requirements to ac-
 215 cept the results:

- 216 1. The angle between the vectors defined by the minimum variance analysis (MVA)
 217 and the magnetic coplanarity method must be less than 15°.
- 218 2. The ratio between the intermediate eigenvalue and the smallest eigenvalue should
 219 be greater than 2, the same for more data points and greater than 10 for data points
 220 less than 50 or the ratio between the smallest eigenvalue to the intermediate eigen-
 221 value should be smaller than 1/3, which is in reverse means greater than 3.

222 These conditions above have been used in previous studies (Facskó et al., 2008, 2009, 2010;
 223 Shan et al., 2013; B. U. O. Sonnerup & Cahill, 1967).

224 5 Observations

225 With the visual inspection of the magnetic field and plasma data, I identified jumps
 226 in magnetic field (\mathbf{B} , speed (\mathbf{V}), density (N), and temperature (T)). Using these quanti-
 227 ties, I determined the times when shocks occurred for each spacecraft data set in each
 228 event. From the plots, the shocks detected by the spacecraft in each event are believed
 229 to be propagation of the same shock due to their timing and the similarities of the mag-
 230 netic field and plasma data profile with one another.

231 The following case studies of two events are not orderly defined for one another.
 232 First, I analyzed the shock event on May 7, 2007, and then the event on April 23, 2007.
 233 Hence, the order follows this fashion.

234 5.1 Event May 7, 2007

235 On May 7, 2007, the Wind spacecraft first detected the shock at 07:02:30 (UTC).
 236 After that, the STEREO–A spacecraft detected the shock at 08:11:30 (UTC), and then
 237 the STEREO–B spacecraft detected the shock at 09:42:00 (UTC). The four Cluster satel-
 238 lites detect the shock as well. Cluster SC1 detected the shock at 08:27:55 (UTC), and
 239 the Cluster SC3 detected the shock at 08:28:00 (UTC). The magnetic field and the plasma
 240 plot are shown in Figure 1 for the Wind, in Figure 2 for the STEREO–A, in Figure 3
 241 for the STEREO–B, in Figure 4 for the Cluster SC1, in Figure 5 for the Cluster SC3.
 242 There is no indication that Cluster SC2 and SC4 detected a shock in the shock database
 243 list. But the four Cluster satellites are much closer together, so they must have detected
 244 the shock. Without plasma data on Cluster SC2 and SC4 satellites, a shock cannot be
 245 confirmed based solely on the magnetic field data. However, using the empirical formula
 246 described in Section 2.4 the electron density could be estimated using EFW spacecraft
 247 potential data. Therefore, comparing the magnetic field and the electron plasma den-
 248 sity profile, the shock is determined. The Cluster-2 spacecraft detected the shock at 08:28:10
 249 (UTC). Figure 6 shows the magnetic field and density plot. The Cluster-4 spacecraft de-
 250 tected the shock at 08:28:10 (UTC). Figure 7 shows the magnetic field and density plot.
 251 Similarly, The electron density parameter is obtained by the empirical formula (Eq. 1).

252 Here we list all magnetic field observations of the spacecraft for the event and ap-
 253 ply the MVA and the CP methods on them. The upstream and downstream time inter-
 254 vals that most agree between the MVA and the CP for all the spacecraft are shown in
 255 Table 1, and their corresponding Figures are 8 for the Wind, 9 for the STEREO–A, 10
 256 for the STEREO–B, 11 for the Cluster SC1, 12 for the Cluster SC3, 13 for the Cluster

257 SC2, and 14 for the Cluster SC4. Table 1 also shows the ratio between the smallest eigen-
 258 value λ_3 and the intermediate eigenvalue λ_2 as well as the angle between the MVA nor-
 259 mal and CP normals in the determined upstream and downstream time intervals for each
 260 spacecraft.

261 The accepted upstream and downstream time intervals are highly accurate consid-
 262 ering the angle difference between the two methods is minimal and the eigenvalue cri-
 263 teria are sufficient for each spacecraft data. Using the determined time intervals, the cal-
 264 culations of the ratio between the upstream and downstream magnetic fields, densities,
 265 and temperatures as well as the bulk speed, and shock θ_{Bn} angle are made. These pa-
 266 rameters, the MVA normal, and the magnetic CP normals are shown in Table 2 and 3.
 267 The shock parameters fulfill the necessary shock criteria (Lumme et al., 2017). The re-
 268 sults of the additional parameters calculations are shown in Table 4 and 5.

269 Using the results, the 2D sketches of the IP shocks that were detected by the space-
 270 craft are shown in Figure 15. In these 2D sketches, the shock propagation and normal
 271 vector orientation are shown in a temporal development manner. Since four Cluster satel-
 272 lites are relatively close to one another, their averaged position as well as normal vec-
 273 tors are shown in the general 2D and 3D sketches. For explicitly showing normal vec-
 274 tor directions and positions of all Clusters satellites, it is suitable to change their coor-
 275 dinates and normal vectors into a GSE coordinate system with the positions in the Earth
 276 radii (R_E) unit, see Figure 16.

277 The 3D sketch is shown in 17, and in the 3D sketch, the STEREO–A, and B, and
 278 averaged Clusters positions are time-shifted to the Wind’s position to see the overall shape
 279 of this IP shock. From the 3D sketch, the overall shape of the IP shock is a planner and
 280 can be fitted with a plane (Figure 17, bottom).

281 5.2 Event April 23, 2007

282 In this specific event STEREO–A spacecraft detected a shock first at 06:53:35 (UTC),
 283 then the ACE spacecraft detected the shock at 08:57:00 (UTC), and the Wind space-
 284 craft detected the shock at 09:12:00 (UTC). The magnetic field and the plasma data are
 285 shown in Figure 18 for the STEREO–A, in Figure 19 for the ACE, and in Figure 20 for
 286 the Wind.

287 STEREO–A and B have identical instruments, therefore, STEREO–B must have
 288 detected the shock on that day even though there is no detected IP shock for STEREO–B
 289 in the shock lists database mentioned in Section 3. So, by using the average solar wind
 290 speed, 400 km/s, we concluded that the shock detection time for STEREO–B should be
 291 around 13:00 to 15:00. Considering this, a could-be shock signature from STEREO–B
 292 is found around 13:21:30 even though it is a faint signature. The magnetic field and the
 293 plasma plot are shown in Figure 21.

294 Here we list all magnetic field observations of the spacecraft for the event and ap-
 295 ply the MVA and the CP methods to them. In this event, the order between upstream
 296 and downstream is swapped because it is a fast-reverse (FR) shock event, which means
 297 the shock is up against its driver. The upstream and downstream time intervals that most
 298 agree between the MVA and the CP for all the spacecraft are shown in Table 6 and their
 299 corresponding Figures are 22 for the STEREO–A, 23 for the ACE, 24 for the Wind, and
 300 25 for the STEREO–B. Table 6 also shows the ratio between the intermediate eigen-
 301 value λ_2 and the smallest eigenvalue λ_3 as well as the angle between the MVA normal
 302 and CP normals in the determined upstream and downstream time intervals for each space-
 303 craft.

304 Similarly to the event about, the upstream and downstream time intervals are highly
 305 accurate as well, considering the angle difference between the two methods is minimal

and the eigenvalue criteria are fulfilled for each spacecraft data. Also, using the determined time intervals, the estimations of the ratio between the upstream and downstream magnetic field, densities, and temperatures as well as the bulk speed, and shock θ_{Bn} angle are made. These parameters, the minimum variance analysis normal and the magnetic coplanarity normal are shown in Table 7, 8, where also the solar wind bulk speed and the downstream to upstream ratios for the shock criteria are fulfilled (Lumme et al., 2017), and the STEREO–B ratios are compatible with the shock criteria, proving that the STEREO–B did detect the shock. However, the shock detected by the STEREO–B appears to become quasi-parallel a few hours after the shock detection times of STEREO–A, ACE, and the Wind based on the shock θ_{Bn} angle, see Table 9 10, where the calculated results of additional parameters are shown.

The sketches of the IP shocks that were detected by the spacecraft are shown on Figure 26. In these 2D sketches, the shock propagation and normal vector orientation are shown in a temporal development manner. The 3D sketch of the IP shock is shown on Figure 27, and in the 3D sketch, the Wind, ACE, and STEREO–B positions are time-shifted to the STEREO–A’s position to see the overall shape of this IP shock.

6 Discussion

The IP shock parameters did not change significantly from STEREO A to B in neither case (Table 2, 3, 4, 5, 7, 8, 9, 10). There is no sign of wave dispersion on the scale of 40 million km. Therefore, this paper is continued as case study based on conjugated multi-spacecraft observation of two IP shcok events.

6.1 Event May 7, 2007

The IP shock fitted plane is tilted 56.42° with respect to the Sun-Earth line according to Figure 17 (bottom). The tilt appears to be almost the same degree as the Parker spiral impacting the Earth from the dawn side. Hence, it is the reason why the Wind detected the shock first even though STEREO–A’s position is relatively closer to the Sun’s direction. This period, 2007, was during the solar minimum phase, and stream interaction region (SIR) or co-rotating stream interactions (CIR) were dominant (Opitz et al., 2014), and this further proves the result, see Figure 28. Furthermore, to see a correlation between fast-forward shock and geomagnetic activity, we determined the K_p -index (Bartels, 1949; Rostoker, 1972; Matzka et al., 2021, <https://www.swpc.noaa.gov/noaa-scales-explanation>) on May 07, 2007, as shown in Figure 29. It appears that this forward shock-leading event disturbed the magnetosphere, causing a G1-minor geomagnetic storm with the K_p - index peaking around 15:00 (UTC). The geomagnetic sub-storm happened about 6 hours after the detection of the shock by the STEREO–B spacecraft.

6.2 Event April 23, 2007

On Figure 27 it seems that the shape of the shock is not uniform and is twisted from the STEREO–A spacecraft to the other three spacecraft in the Z-axis along the transverse direction (Y-axis) to the Sun-Earth line, see Figure 27, (top right). As seen from Figure 27 (bottom), the STEREO–A alone is on the dusk (left) side of the Sun-Earth line while the Wind, the ACE, and the STEREO–B are on the dawn (right). In this XY-plane view, the shock normal vectors appear to be changing or slightly rotating their direction from the STEREO–A to the Wind, the ACE, and the STEREO–B along Y-axis, and the shock is changing from the quasi-perpendicular to quasi-parallel based on the shock θ_{Bn} angle. This IP shock is a fast reverse shock, meaning it travels toward the Sun even though the shock propagates away from the Sun with the solar wind. The shock detection time between the STEREO–A and the Wind/ACE is about two hours while

354 the between STEREO–A and B is almost six hours, yet the shock orientation is signif-
 355 icantly changed from the STEREO–A to the other three spacecraft indicating the change
 356 is spatial, not temporal. So, due to this nature, the IP shock could be a local ripple. The
 357 ripples on the shock surface are known for being caused by ICME (interplanetary coro-
 358 nal mass ejections) shock drivers as they do not propagate into homogeneous interplan-
 359 etary medium (Acuña et al., 2008). However, the source of this event is a stream-interaction
 360 region (SIR) as listed here https://stereo-ssc.nascom.nasa.gov/pub/ins_data/impact/level3/STEREO_Level3_Shock.pdf.
 361

362 We determined the K_p -index of this event as seen in Figure 30. Similar to the fast-
 363 forward shock event of May 07, 2007, a G1-minor geomagnetic storm occurred on this
 364 day, but the beginning of the geomagnetic storm happened three hours before the shock
 365 detection time of the STEREO–A while the ending of the storm was partially at the same
 366 time as the STEREO–A. As stated before, SIR/CIRs form when the fast-moving solar
 367 wind catches the slow-moving solar wind (Richardson, 2018). This sometimes forms a
 368 pair of shocks, one leading as a fast-forward shock while a rarefied shock trails the so-
 369 lar wind as a fast-reverse shock but oftentimes as just sole fast-forward or fast reverse
 370 shocks (Jian et al., 2019). Nevertheless, since it always involves the fast-moving solar wind,
 371 it makes total sense why the G1-minor geomagnetic storm with a K_p -5 index happened
 372 before the detection of the shock because it seems the fast-moving solar wind caused the
 373 minor storm before the fast-reverse shock finally arrived at the spacecraft positions.

374 The normal orientation inconsistency can also be explained by the argument that
 375 this shock is a fast-reverse shock because SIRs have characteristic tilts such that forward
 376 waves direct towards the solar equatorial plane while the reverse waves tend to move in
 377 the direction of the solar poles (Kilpua et al., 2015). Therefore, this tilting nature may
 378 explain the XZ component tilted orientation between the STEREO–A and the other three
 379 spacecraft – the Wind, the ACE, and the STEREO–B.

380 7 Summary and conclusions

381 In this paper, two conjugated multi-spacecraft studies of the interplanetary (IP)
 382 shock propagation are presented. Its purpose is to determine how IP shocks are devel-
 383 oping and evolving in spatial and temporal propagation. For this purpose, two methods
 384 are implemented, namely the minimum variance analysis of the magnetic field (MVA)
 385 and the magnetic coplanarity methods (CP) for the determination of upstream and down-
 386 stream time intervals. The two methods use magnetic field measurement data, which is
 387 known for its high resolutions compared to those of plasma data concerning their respec-
 388 tive heliospheric variational rates. To acquire data, we used the Coordinated Data Anal-
 389 ysis Web (CDAWeb) of NASA for each spacecraft. Data are in the first event case – from
 390 early morning to noon in on May 7, 2007 for seven different spacecraft, namely Wind,
 391 Stereo A and B, and 4 Cluster satellites.

392 The second event case, similarly, - from early morning to noon in April 23, 2007
 393 for four different spacecraft, namely Wind, STEREO–A and B, and ACE. After acquir-
 394 ing data, we tranformed the data to the HEE coordinate system so that it is easy to com-
 395 pare the data and how the shock parameters change when propagating through space.
 396 However, near Earth, vectors are changed to the GSE coordinate system. For accept-
 397 ing the upstream and downstream time intervals, two criteria are made such as the θ
 398 angle differences between MVA and the magnetic coplanarity must be considerably small,
 399 $< 15^\circ$, and the ratio between the intermediate eigenvalue to the smallest eigenvalue must
 400 be greater than 3. For both case studies, we found such upstream and downstream in-
 401 tervals, indicating the results are highly accurate. Hence, pinpointing the shock forma-
 402 tions has been very successful due to using the two methods to determine the shock nor-
 403 mal vectors.

404 The two event studies are not timely ordered. First, the Event May 7, 2007, is studied,
 405 and then the Event April 23, 2007, is followed. Therefore, the Event May 7 is referred
 406 to as the first event and the Event April 23 is the second event. The first event
 407 is a fast-forward (FF) shock event, the shock propagating away from the Sun in the solar
 408 wind frame of reference in addition to the solar wind on which it propagates is also
 409 traveling away from the Sun. The shock parameters agree within the errors. From the
 410 2D sketches as well as the 3D sketch, on which the positions of the STEREO–A and B,
 411 and 4 Clusters spacecraft are time-shifted to the shock detection time of the Wind space-
 412 craft to see the geometry of the shock, the shock appears planar and tilted 56.42° to the
 413 Sun-Earth line, explaining why the Wind first detected the IP shock even though its lo-
 414 cation is behind the STEREO–A in respect to the Sun-Earth line. The tilt of this pla-
 415 nar shock surface is almost identical to the usual propagation of the Parker spiral im-
 416 pacting the Earth. Consequently, this indicates the origin of the shock is co-rotating stream
 417 interactions (CIRs), which agrees with the detected CIR on that day. There is no sign
 418 of temporal change in this scale. In the spatial range of 40 million km, no change was
 419 observable. The G1-minor geomagnetic storm happened after this shock was detected,
 420 indicating this shock event caused the geomagnetic storm on that day.

421 The second event is the fast reverse (FR) shock event, the shock propagates toward
 422 the Sun in the solar wind frame of reference although the shock propagates away from
 423 the Sun with its carrier solar wind. There are several peculiarities with this shock event,
 424 it appears the shape of the shock is not uniform and twisted from the STEREO–A space-
 425 craft to the other spacecraft along the transverse direction to the Sun-Earth line. The
 426 shock normal vectors also were observed to be changing along Y-axis. A G1-minor ge-
 427 oomagnetic storm occurred on this day, similar to the fast-forward shock event of May
 428 7, 2007. Intriguingly, the onset of this storm took place three hours prior to the shock
 429 detection time recorded by STEREO–A. The termination of the storm partially coin-
 430 cided with the STEREO–A detection time. The formation of Stream Interaction Re-
 431 gions/Corotating Interaction Regions (SIR/CIRs) occurs when a faster solar wind stream
 432 encounters a slower one. The source of this shock is SIR/CIR.

433 Given the involvement of fast-moving solar wind, it's logical that the G1-minor ge-
 434 omagnetic storm, with a K_p -5 index, began before the shock detection. It appears that
 435 the fast-moving solar wind instigated the minor storm prior to the arrival of the fast-
 436 reverse shock at the spacecraft's position.

437 The orientation irregularity can be potentially accounted for by the characteris-
 438 tic tilts of SIRs. The forward waves of SIRs tend to propagate towards the solar equa-
 439 torial plane, while the reverse waves lean towards the solar poles. This inherent tilting
 440 could explain the tilted orientation of the XZ component observed between the STEREO–A
 441 and the other three spacecraft – Wind, ACE, and STEREO–B. Even without this char-
 442 acteristic tilting, the fast-reverse shock is being compressed, which, given its defining na-
 443 ture, could explain the irregularities.

444 Acknowledgments

445 We would also like to acknowledge NASA CDAWeb, the STEREO–A and B IMPACT,
 446 PLASTIC, the Wind MFI, SWE, ACE MAG, SWEPAM, and the Cluster FGM, CIS,
 447 EFW teams for providing data, comprehensive Heliospheric Shock Database (ipshocks.fi)
 448 developed and hosted at University of Helsinki for the main data selection process, and
 449 TREPS, designed and developed by the French Plasma Physics Data Centre (CDPP),
 450 for coordinate transformations for this study. This work was partially financed by the
 451 National Research, Development, and Innovation Office (NKFIH) FK128548 grant. ML
 452 was supported by the Stipendium Hungaricum Scholarship.

453 **References**

- 454 Acuña, M. H., Curtis, D., Scheifele, J. L., Russell, C. T., Schroeder, P., Szabo,
 455 A., & Luhmann, J. G. (2008, April). The STEREO/IMPACT Magnetic
 456 Field Experiment. *Space Science Reviews*, 136(1-4), 203-226. doi:
 457 10.1007/s11214-007-9259-2
- 458 Balogh, A., Dunlop, M. W., Cowley, S. W. H., Southwood, D. J., Thomlinson,
 459 J. G., Glassmeier, K. H., ... Kivelson, M. G. (1997, January). The Cluster
 460 Magnetic Field Investigation. *Space Science Reviews*, 79, 65-91. doi:
 461 10.1023/A:1004970907748
- 462 Bartels, J. (1949). The standardized index ks, and the planetary index kp, iatme
 463 bull., 12 (b), 97; iugg publ. *Office, Paris*.
- 464 Biermann, L. (1957, June). Solar corpuscular radiation and the interplanetary gas.
 465 *The Observatory*, 77, 109-110.
- 466 Cid, C., Palacios, J., Saiz, E., Guerrero, A., & Cerrato, Y. (2014, October). On
 467 extreme geomagnetic storms. *Journal of Space Weather and Space Climate*, 4,
 468 A28. doi: 10.1051/swsc/2014026
- 469 CIS team. (2021). *Cluster active archive: Cis user guide*. https://caa.esac.esa.int/documents/UG/CAA_EST_UG_CIS_v37.pdf.
- 470 Escoubet, C. P., Fehringer, M., & Goldstein, M. (2001, October). Introduction: The
 471 Cluster mission. *Annales Geophysicae*, 19, 1197-1200. doi: 10.5194/angeo-19
 472 -1197-2001
- 473 Facskó, G., Kecskeméty, K., Erdős, G., Tátrallyay, M., Daly, P. W., & Dan-
 474 douras, I. (2008, January). A statistical study of hot flow anomalies us-
 475 ing Cluster data. *Advances in Space Research*, 41(8), 1286-1291. doi:
 476 10.1016/j.asr.2008.02.005
- 477 Facskó, G., Németh, Z., Erdos, G., Kis, A., & Dandouras, I. (2009, May). A global
 478 study of hot flow anomalies using Cluster multi-spacecraft measurements. *An-
 479 nales Geophysicae*, 27(5), 2057-2076. doi: 10.5194/angeo-27-2057-2009
- 480 Facskó, G., Trotignon, J. G., Dandouras, I., Lucek, E. A., & Daly, P. W. (2010,
 481 February). Study of hot flow anomalies using Cluster multi-spacecraft mea-
 482 surements. *Advances in Space Research*, 45(4), 541-552. doi: 10.1016/
 483 j.asr.2009.08.011
- 484 Galvin, A. B., Kistler, L. M., Popecki, M. A., Farrugia, C. J., Simunac, K. D. C.,
 485 Ellis, L., ... Steinfeld, D. (2008, April). The Plasma and Suprathermal Ion
 486 Composition (PLASTIC) Investigation on the STEREO Observatories. *Space
 487 Science Reviews*, 136(1-4), 437-486. doi: 10.1007/s11214-007-9296-x
- 488 Génot, V., Renard, B., Dufourg, N., Bouchemit, M., Lormant, N., Beigbeder, L., ...
 489 Gangloff, M. (2018, January). TREPS, a tool for coordinate and time trans-
 490 formations in space physics. *Planetary and Space Science*, 150, 86-90. doi:
 491 10.1016/j.pss.2017.06.002
- 492 Gonzalez, W. D., Joselyn, J. A., Kamide, Y., Kroehl, H. W., Rostoker, G., Tsu-
 493 rutani, B. T., & Vasylunas, V. M. (1994, April). What is a geomag-
 494 netic storm? *Journal of Geophysical Research*, 99(A4), 5771-5792. doi:
 495 10.1029/93JA02867
- 496 Gustafsson, G., Bostrom, R., Holback, B., Holmgren, G., Lundgren, A., Stasiewicz,
 497 K., ... Wygant, J. (1997, January). The Electric Field and Wave Experi-
 498 ment for the Cluster Mission. *Space Science Reviews*, 79, 137-156. doi:
 499 10.1023/A:1004975108657
- 500 Jian, L. K., Luhmann, J. G., Russell, C. T., & Galvin, A. B. (2019, March). Solar
 501 Terrestrial Relations Observatory (STEREO) Observations of Stream Inter-
 502 action Regions in 2007 - 2016: Relationship with Heliospheric Current Sheets,
 503 Solar Cycle Variations, and Dual Observations. *Solar Physics*, 294(3), 31. doi:
 504 10.1007/s11207-019-1416-8
- 505 Jyothi, S. A. (2021). Solar superstorms: Planning for an internet apocalypse. In
 506 *Proceedings of the 2021 acm sigcomm 2021 conference* (p. 692-704). New York,

- 508 NY, USA: Association for Computing Machinery. Retrieved from <https://doi.org/10.1145/3452296.3472916> doi: 10.1145/3452296.3472916
- 509 Kaiser, M. L., & Adams, W. J. (2007). Stereo mission overview. In *2007 ieee aerospace conference* (pp. 1–8).
- 510 Kaiser, M. L., Kucera, T. A., Davila, J. M., St. Cyr, O. C., Guhathakurta, M., & Christian, E. (2008, April). The STEREO Mission: An Introduction. *Space Science Reviews*, 136(1-4), 5-16. doi: 10.1007/s11214-007-9277-0
- 511 Keith, W., & Heikkila, W. (2021). 1 - historical introduction. In W. Keith & W. Heikkila (Eds.), *Earth's magnetosphere (second edition)* (Second Edition ed., p. 1-88). Academic Press. Retrieved from <https://www.sciencedirect.com/science/article/pii/B9780128181607000016> doi: <https://doi.org/10.1016/B978-0-12-818160-7.00001-6>
- 512 Kilpua, E. K. J., Lumme, E., Andreeova, K., Isavnin, A., & Koskinen, H. E. J. (2015, June). Properties and drivers of fast interplanetary shocks near the orbit of the Earth (1995–2013). *Journal of Geophysical Research (Space Physics)*, 120(6), 4112-4125. doi: 10.1002/2015JA021138
- 513 Lepping, R. P., Acuña, M. H., Burlaga, L. F., Farrell, W. M., Slavin, J. A., Schatten, K. H., ... Worley, E. M. (1995, February). The Wind Magnetic Field Investigation. *Space Science Reviews*, 71(1-4), 207-229. doi: 10.1007/BF00751330
- 514 Lumme, E., Kilpua, E., Isavnin, A., & Andreeova, K. (2017). *Database of heliospheric shock waves* (Tech. Rep.). University of Helsinki.
- 515 Matzka, J., Stolle, C., Yamazaki, Y., Bronkalla, O., & Morschhauser, A. (2021, May). The Geomagnetic Kp Index and Derived Indices of Geomagnetic Activity. *Space Weather*, 19(5), e2020SW002641. doi: 10.1029/2020SW002641
- 516 McComas, D. J., Bame, S. J., Barker, P., Feldman, W. C., Phillips, J. L., Riley, P., & Griffee, J. W. (1998, July). Solar Wind Electron Proton Alpha Monitor (SWEPAM) for the Advanced Composition Explorer. *Space Science Reviews*, 86, 563-612. doi: 10.1023/A:1005040232597
- 517 NASA WIND team. (2020). *Wind spacecraft*. (<https://wind.nasa.gov/>)
- 518 NASA WIND team. (2022). *Wind data sources*. https://wind.nasa.gov/data_sources.php.
- 519 Ogilvie, K. W., Chornay, D. J., Fritzenreiter, R. J., Hunsaker, F., Keller, J., Lobell, J., ... Gergin, E. (1995, February). SWE, A Comprehensive Plasma Instrument for the Wind Spacecraft. *Space Science Reviews*, 71(1-4), 55-77. doi: 10.1007/BF00751326
- 520 Opitz, A., Sauvaud, J.-A., Klassen, A., Gomez-Herrero, R., Bucik, R., Kistler, L. M., ... Lavraud, B. (2014, August). Solar wind control of the terrestrial magnetotail as seen by STEREO. *Journal of Geophysical Research (Space Physics)*, 119(8), 6342-6355. doi: 10.1002/2014JA019988
- 521 Organization, W. M. (2021). *Fluxgate magnetometer (fgm)*. <https://space.oscar.wmo.int/instruments/view/fgm>. Retrieved from <https://space.oscar.wmo.int/instruments/view/fgm> (OSCAR Space)
- 522 Parker, E. N. (1958, November). Dynamics of the Interplanetary Gas and Magnetic Fields. *The Astrophysical Journal*, 128, 664. doi: 10.1086/146579
- 523 Paschmann, G., & Daly, P. W. (1998, January). Analysis Methods for Multi-Spacecraft Data. ISSI Scientific Reports Series SR-001, ESA/ISSI, Vol. 1. ISBN 1608-280X, 1998. *ISSI Scientific Reports Series*, 1.
- 524 Reme, H., Bosqued, J. M., Sauvaud, J. A., Cros, A., Dandouras, J., Aoustin, C., ... Balsiger, H. (1997, January). The Cluster Ion Spectrometry (cis) Experiment. *Space Science Reviews*, 79, 303-350. doi: 10.1023/A:1004929816409
- 525 Richardson, I. G. (2018, January). Solar wind stream interaction regions throughout the heliosphere. *Living Reviews in Solar Physics*, 15(1), 1. doi: 10.1007/s41116-017-0011-z
- 526 Rostoker, G. (1972, January). Geomagnetic indices. *Reviews of Geophysics and*

- Space Physics, 10, 935-950. doi: 10.1029/RG010i004p00935

Sandhu, J. K., Yeoman, T. K., Fear, R. C., & Dandouras, I. (2016, November). A statistical study of magnetosospheric electron density using the Cluster spacecraft. *Journal of Geophysical Research (Space Physics)*, 121(11), 11,042-11,062. doi: 10.1002/2016JA023397

Schwartz, S. J. (1998, January). Shock and Discontinuity Normals, Mach Numbers, and Related Parameters. *ISSI Scientific Reports Series*, 1, 249-270.

Shan, L., Lu, Q., Zhang, T., Gao, X., Huang, C., Su, Y., & Wang, S. (2013, February). Comparison between magnetic coplanarity and MVA methods in determining the normal of Venusian bow shock. *Chinese Science Bulletin*, 201, 1-4. doi: 10.1007/s11434-013-5675-8

Smith, C. W., L'Heureux, J., Ness, N. F., Acuña, M. H., Burlaga, L. F., & Scheifele, J. (1998, July). The ACE Magnetic Fields Experiment. *Space Science Reviews*, 86, 613-632. doi: 10.1023/A:1005092216668

Snyder, C. W., & Neugebauer, M. (1965, January). Interplanetary Solar-Wind Measurements by Mariner II. In C. C. Chang & S. S. Huang (Eds.), *Plasma space science* (Vol. 3, p. 67). doi: 10.1007/978-94-011-7542-5_8

Sonnerup, B. U. O., & Cahill, J., L. J. (1967, January). Magnetopause Structure and Attitude from Explorer 12 Observations. *Journal of Geophysical Research*, 72, 171. doi: 10.1029/JZ072i001p00171

Sonnerup, B. U. Ö., & Scheible, M. (1998, January). Minimum and Maximum Variance Analysis. *ISSI Scientific Reports Series*, 1, 185-220.

Stone, E. C., Frandsen, A. M., Mewaldt, R. A., Christian, E. R., Margolies, D., Ormes, J. F., & Snow, F. (1998, July). The Advanced Composition Explorer. *Space Science Reviews*, 86, 1-22. doi: 10.1023/A:1005082526237

Trottignon, J. G., Décréau, P. M. E., Rauch, J. L., Vallières, X., Rochel, A., Kouglénou, S., ... Masson, A. (2010). The WHISPER Relaxation Sounder and the CLUSTER Active Archive. *Astrophysics and Space Science Proceedings*, 11, 185-208. doi: 10.1007/978-90-481-3499-1__12

Trottignon, J.-G., Vallières, & the WHISPER team. (2011). *Calibration report of the whisper measurements in the cluster active archive (caa)* (Tech. Rep.). LPC2E CNRS. (caa-est-cr-whi)

Tsurutani, B. T., & Lin, R. P. (1985, January). Acceleration of >47 keV ions and >2 keV electrons by interplanetary shocks at 1 AU. *Journal of Geophysical Research*, 90(A1), 1-11. doi: 10.1029/JA090iA01p00001

Wilson, I., Lynn B., Brosius, A. L., Gopalswamy, N., Nieves-Chinchilla, T., Szabo, A., Hurley, K., ... TenBarge, J. M. (2021, May). A Quarter Century of Wind Spacecraft Discoveries. *Reviews of Geophysics*, 59(2), e2020RG000714. doi: 10.1029/2020RG000714

Zhang, J. C., Kistler, L. M., Mouikis, C. G., Dunlop, M. W., Klecker, B., & Sauvaud, J. A. (2010, June). A case study of EMIC wave-associated He⁺ energization in the outer magnetosphere: Cluster and Double Star 1 observations. *Journal of Geophysical Research (Space Physics)*, 115(A6), A06212. doi: 10.1029/2009JA014784

Table 1. Here, Δt_{up} denotes the defined upstream and Δt_{down} denotes the defined downstream time intervals with minimum variance (MVA) and magnetic co-planarity (CP) analysis methods. λ_2/λ_3 indicates the ratio between the intermediate eigenvalue λ_2 and the smallest eigenvalue λ_3 , and $\Delta\theta_{MVA-CP}$ is the angle between the MVA and CP normals.

Spacecraft	Δt_{up} [hh:mm:ss-hh:mm:ss]	Δt_{down} [hh:mm:ss-hh:mm:ss]	λ_2/λ_3	$\Delta\theta_{MVA-CP}$ [°]
Wind	06:59:00 - 07:01:47	07:03:50 - 07:05:50	14.82	0.38
STEREO-A	08:08:00 - 08:10:05	08:12:30 - 08:13:50	3.16	0.37
STEREO-B	09:37:00 - 09:40:35	09:42:57 - 09:43:38	9.51	1.10
Cluster-1	08:26:10 - 08:27:00	08:28:00 - 08:29:00	167.90	0.21
Cluster-3	08:26:30 - 08:27:10	08:29:00 - 08:29:47	22.43	1.92
Cluster-2	08:26:56 - 08:27:40	08:28:32 - 08:29:37	91.56	0.10
Cluster-4	08:26:25 - 08:27:10	08:28:45 - 08:29:40	238.63	2.49

Table 2. Resulting core parameters of studying the data of the Wind, STEREO–A, B, and Cluster spacecraft. Here θ_{Bn} is the shock θ angle. The values with the asterisk (*) symbol indicate the parameters with indefinite uncertainties because the determined intervals of the upstream and downstream magnetic fields are smaller than the resolution of the plasma data. Due to the CIS experiment is not operational for Cluster SC2, and the CIS HIA subinstrument being switched off for Cluster SC4 spacecraft, the plasma parameters are not available for these satellites. The Cluster CIS HIA instruments SC1 and SC3 provide parallel (T_{\parallel}) and perpendicular (T_{\perp}) temperatures, respectively.

Spacecraft	B_d/B_u	N_d/N_u	T_d/T_u	ΔV [km/s]	θ_{Bn} $^{\circ}$
Wind	1.86 ± 0.10	1.78^*	1.33^*	29.60^*	70.80
STEREO–A	1.89 ± 0.02	2.18 ± 0.90	3.21 ± 2.4	36.00 ± 6.00	81.83
STEREO–B	1.90 ± 0.07	1.90 ± 0.6	2.90 ± 6.00	40.25 ± 11.00	59.45
Cluster 1	1.53 ± 0.04	1.63 ± 0.09	$1.10_{\parallel} \pm 1.30_{\parallel}$ $1.40_{\perp} \pm 0.32_{\perp}$	31.20 ± 3.10	86.62
Cluster 3	1.57 ± 0.05	1.69 ± 0.08	$1.20_{\parallel} \pm 1.50_{\parallel}$ $1.40_{\perp} \pm 0.40_{\perp}$	30.50 ± 2.80	89.74
Cluster 2	1.53 ± 0.03	1.42 ± 0.18	NaN	NaN	88.19
Cluster 4	1.57 ± 0.05	1.49 ± 0.19	NaN	NaN	86.55

Table 3. Resulting core parameters of studying the data of the Wind, STEREO–A, B and, Cluster spacecraft. Here $\Delta\theta_{MVA-CP}$ is difference of the normals provided by the minimum variance analysis (MVA) and the co-planarity (CP) methods.

Spacecraft	MVA	CP	$\Delta\theta_{MVA-CP}$
Wind	[-0.76, -0.63, -0.14]	[-0.76, -0.63, -0.15]	0.37
STEREO–A	[0.89, 0.44, 0.14]	[0.89, 0.44, 0.144]	0.38
STEREO–B	[-0.85 -0.51 -0.09]	[-0.86 -0.50 -0.08]	1.10
Cluster-1	[0.85 0.53 -0.03]	[-0.85 -0.53 -0.03]	0.21
Cluster-3	[0.75 0.64 0.15]	[-0.76 -0.63 -0.12]	1.92
Cluster-2	[0.84 0.54 0.01]	[-0.84 -0.54 -0.01]	0.10
Cluster-4	[0.86 0.51 -0.08]	[0.84 0.53 0.11]	2.49

Table 4. Resulting additional parameters of studying the data of the three spacecraft. V_{sh} is the shock speed, C_s^{up} is the upstream sound speed, V_A^{up} is the upstream Alfvén speed, and C_{ms}^{up} is the upstream magnetosonic speed.

Spacecraft	V_{sh} [km/s]	C_s^{up} [km/s]	V_A^{up} [km/s]	C_{ms}^{up} [km/s]
Wind	313.60	47.20 ± 1.60	18.70 ± 6.08	50.78 ± 2.70
STEREO-A	352.41	46.27 ± 3.30	34.89 ± 15.00	57.95 ± 9.41
STEREO-B	354.91	46.89 ± 5.85	31.95 ± 7.33	56.74 ± 6.35
Cluster 1	342.02	43.88 ± 3.09	25.59 ± 7.70	51.31 ± 3.99
Cluster 3	308.11	43.88 ± 2.63	26.80 ± 7.64	51.42 ± 3.98

Table 5. Resulting additional parameters of studying the data of the three spacecraft. Plasma β_{up} based on upstream parameters, Alfvén-Mach (M_A), and Magnetosonic-Mach (M_{ms}) numbers are shown.

Spacecraft	Plasma β_{up}	M_A	M_{ms}
Wind	7.60 ± 4.90	4.14 ± 1.72	1.50 ± 0.40
STEREO-A	2.11 ± 1.80	2.19 ± 1.12	1.32 ± 0.42
STEREO-B	2.58 ± 1.34	2.76 ± 1.07	1.55 ± 0.52
Cluster-1	3.26 ± 1.89	3.84 ± 1.40	1.99 ± 0.46
Cluster-3	3.21 ± 1.83	3.72 ± 1.35	1.93 ± 0.46

Table 6. Here, Δt_{down} denotes the defined downstream and Δt_{up} denotes the defined upstream time intervals with minimum variance (MVA) and co-planarity (CP) analysis methods. λ_3/λ_2 indicates the ratio between the intermediate eigenvalue λ_2 and the smallest eigenvalue λ_2 , and $\Delta\theta_{MVA-CP}$ is the angle between the MVA and CP normals.

Spacecraft	Δt_{down} [hh:mm:ss-hh:mm:ss]	Δt_{up} [hh:mm:ss-hh:mm:ss]	λ_2/λ_3	$\Delta\theta_{MVA-CP}$ [°]
STEREO-A	(06:46:00 - 06:52:23)	(06:57:03 - 07:02:34)	3.29	1.07
ACE	(08:51:30 - 08:56:30)	(09:03:00 - 09:07:00)	4.22	3.43
Wind	(09:04:00 - 09:10:00)	(09:12:20 - 09:13:15)	3.38	1.46
STEREO-B	(13:15:45 - 13:20:00)	(13:24:00 - 13:26:00)	8.18	1.67

Table 7. Resulting core parameters of studying the data of the STEREO–A, B, ACE, and Wind spacecraft. Here θ_{Bn} is the shock θ angle.

Spacecraft	B_d/B_u	N_d/N_u	T_d/T_u	ΔV [km/s]	θ_{Bn} $^{\circ}$
STEREO–A	1.470 ± 0.16	2.000 ± 0.70	1.480 ± 0.50	46.00 ± 13	88.40
ACE	1.410 ± 0.08	1.440 ± 0.16	1.220 ± 0.09	23.720 ± 5.57	46.2
Wind	1.349 ± 0.06	1.424 ± 0.40	1.285 ± 0.7	19.26 ± 0.13	61.85
STEREO–B	1.730 ± 0.09	1.980 ± 0.14	1.340 ± 0.15	21.20 ± 3.4	29.39

Table 8. STEREO–A, B, ACE, and Wind spacecrafts. θ_{MVA-CP} is the angle difference between the minimum variance (MVA) and the magnetic co-planarity (CP) normal vectors.

Spacecraft	MVA	Coplanarity	$\Delta\theta_{MVA-CP}$ °
STEREO–A	[-0.86, 0.02, -0.50]	[-0.86, 0.01, -0.51]	1.07
ACE	[0.87, -0.19, -0.45]	[0.87, -0.23, -0.43]	2.65
Wind	[-0.82, 0.43, 0.37]	[-0.81, 0.44, 0.39]	1.35
STEREO–B	[-0.75, 0.59, 0.29]	[-0.73, 0.61, -0.30]	1.67

Table 9. Resulting additional parameters of studying the data of the three spacecraft. V_{sh} is the shock speed, C_s^{up} is the upstream sound speed, V_A^{up} is the upstream Alfvén-speed and C_{ms}^{up} is the upstream magnetosonic speed.

Spacecraft	V_{sh} km/s	C_s^{up} km/s	V_A^{up} km/s	C_{ms}^{up} km/s
STEREO-A	467.95	64.97 ± 7.74	68.71 ± 29.20	94.57 ± 21.85
ACE	412.36	58.28 ± 4.94	52.82 ± 15.90	78.66 ± 11.26
Wind	372.59	56.14 ± 5.36	56.22 ± 14.71	79.45 ± 11.08
STEREO-B	370.31	57.31 ± 5.38	29.04 ± 12.28	64.25 ± 07.34

Table 10. (Resulting additional parameters of studying the data of the three spacecraft. Plasma β_{up} , Alfvén–Mach number, and Magnetosonic Mach number are shown.

Spacecraft	Plasma β_{up}	Alfvén-Mach	Magnetosonic-Mach
STEREO-A	1.07 ± 0.94	1.00 ± 0.67	0.72 ± 0.41
ACE	1.46 ± 0.91	1.49 ± 0.56	1.00 ± 0.27
Wind	1.19 ± 0.66	1.24 ± 0.52	0.88 ± 0.31
STEREO-B	4.67 ± 4.04	1.69 ± 1.08	0.76 ± 0.37

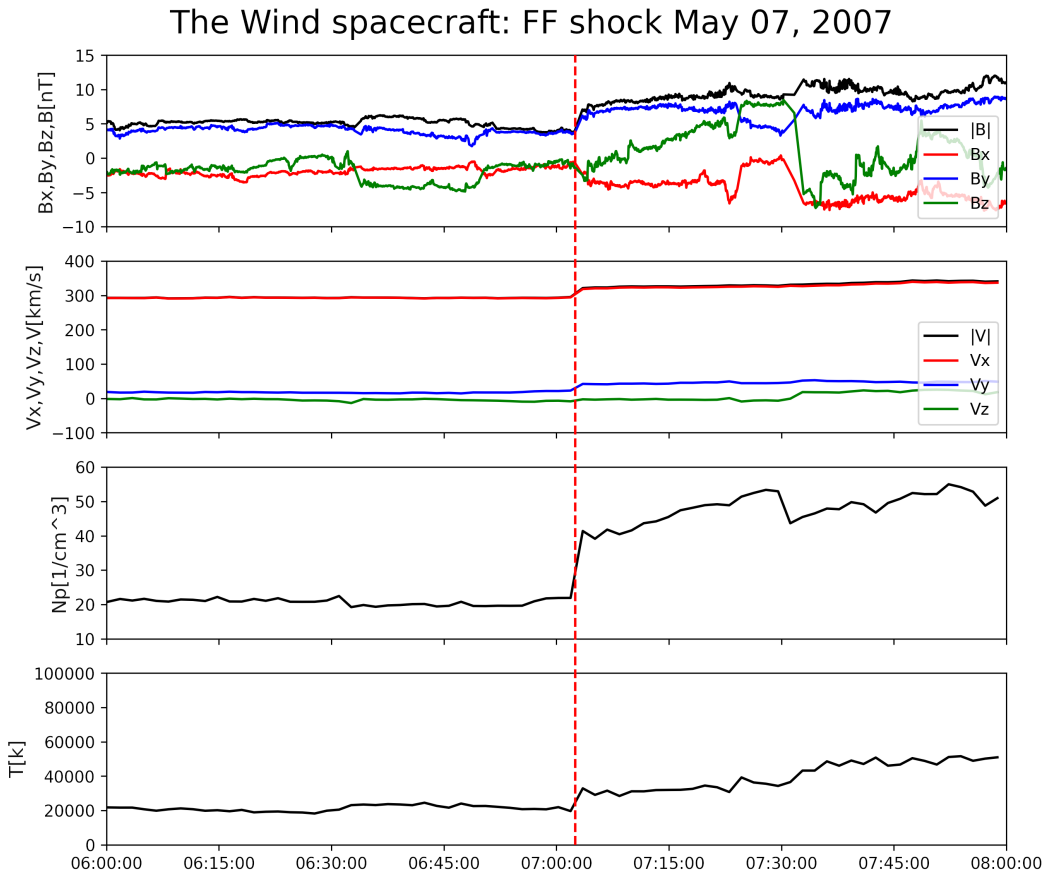


Figure 1. The plot of the shock detected by the Wind spacecraft on May 7, 2007, at 07:02:30 (UTC). FF stands for the fast forward shock, which means the shock is traveling away from its driver. The panels show from top to bottom, the magnetic field magnitude as well as its components, the total velocity, and its components, density, and temperature. The dashed red line represents the exact shock time. The duration of the plot is two hours.

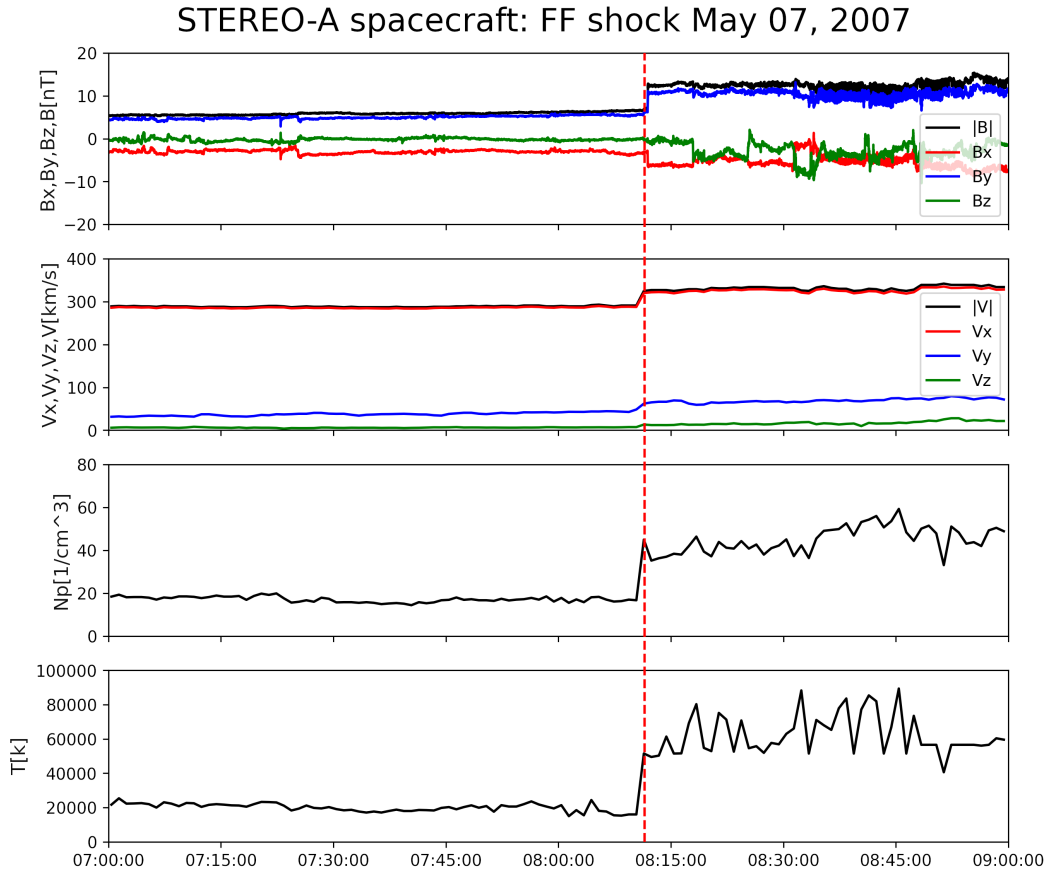


Figure 2. The plot of the shock detected by the STEREO–A spacecraft on May 7, 2007, at 08:11:30 (UTC). The symbols and details of the figures are the same as 1. The duration of the plot is two hours.

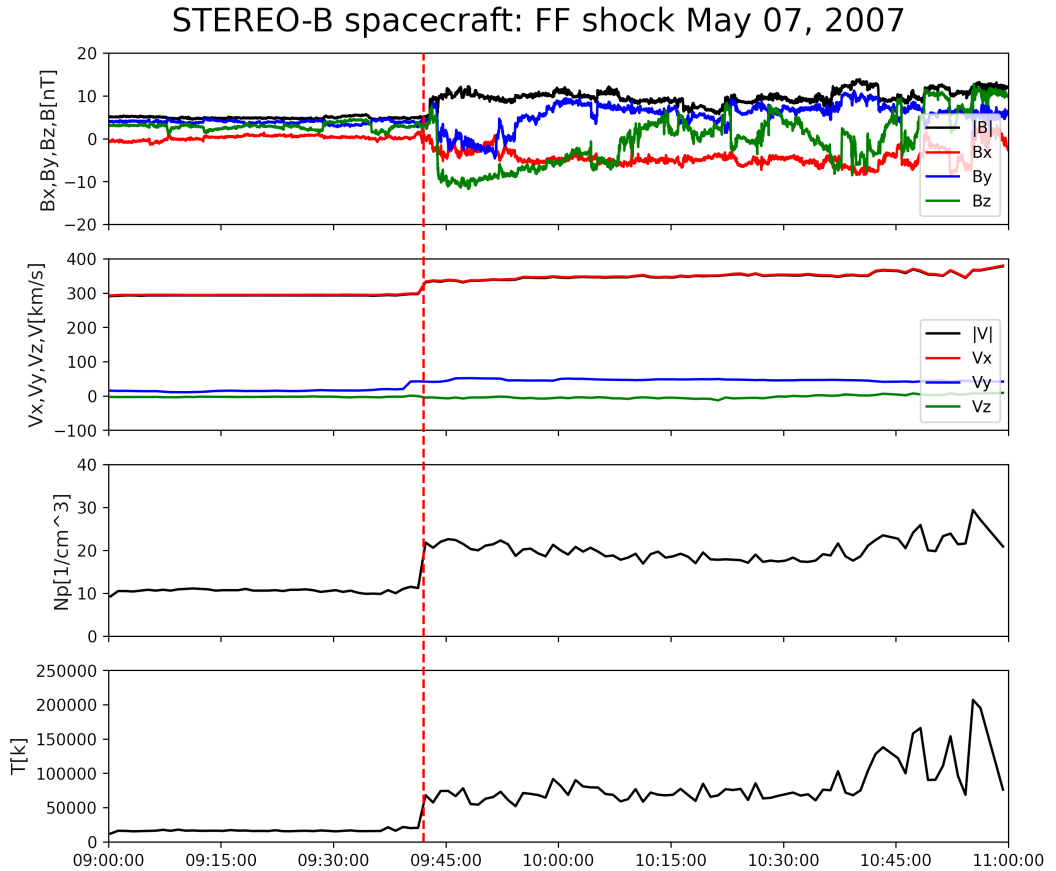


Figure 3. The plot of the shock detected by the STEREO–B spacecraft on May 7, 2007, at 09:42:00 (UTC). The symbols and details of the figures are the same as 1. The duration of the plot is two hours.

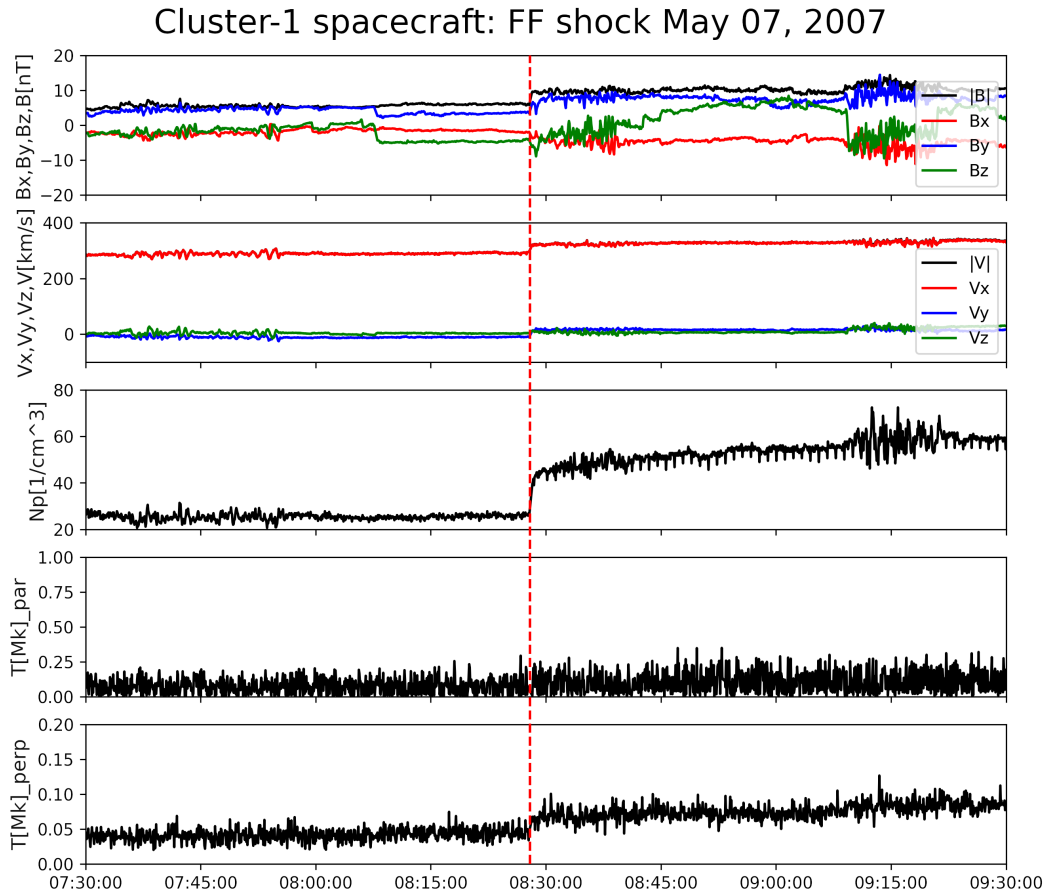


Figure 4. The plot of the shock detected by the Cluster SC1 on May 7, 2007, at 08:27:55 (UTC). The panels show from top to bottom, the magnetic field magnitude as well as its components, the total velocity, and its components, density, and parallel and perpendicular temperatures. The dashed red line represents the exact shock time. The duration of the plot is two hours.

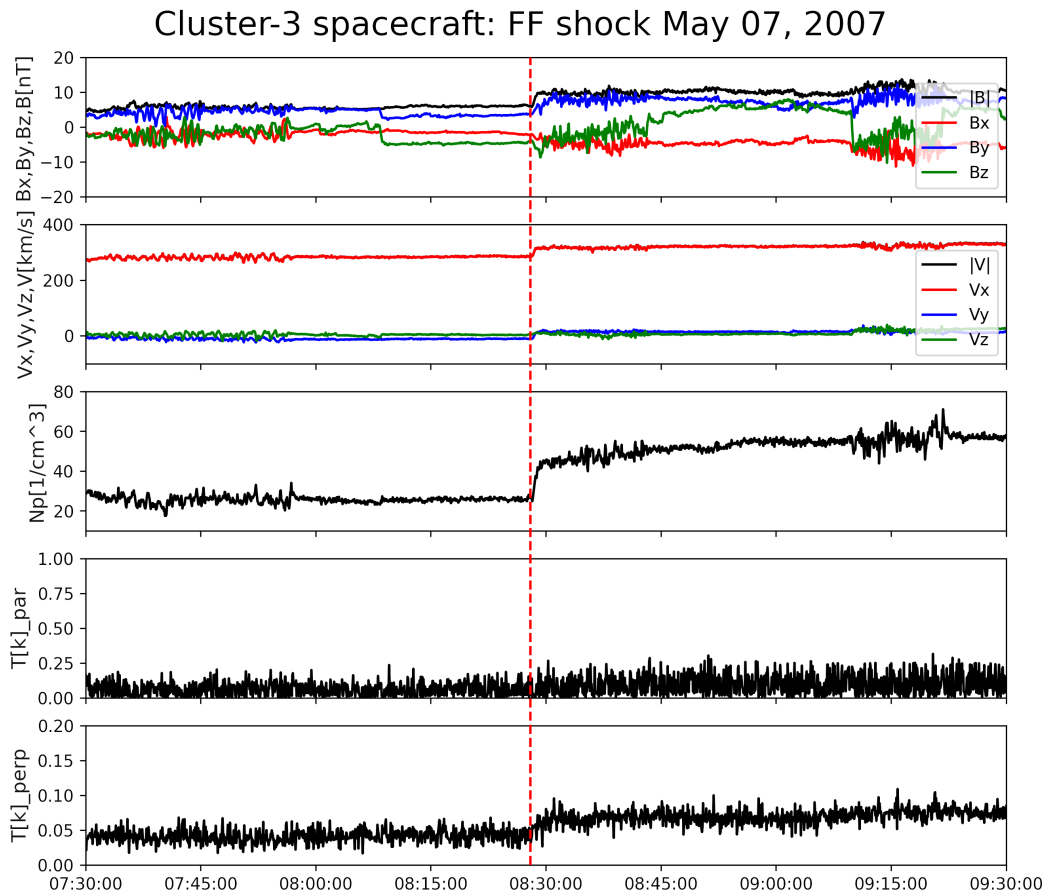


Figure 5. The plot of the shock detected by the Cluster SC3 on May 7, 2007, at 08:28:00 (UTC). The symbols and details of the figures are the same as 4. The duration of the plot is two hours.

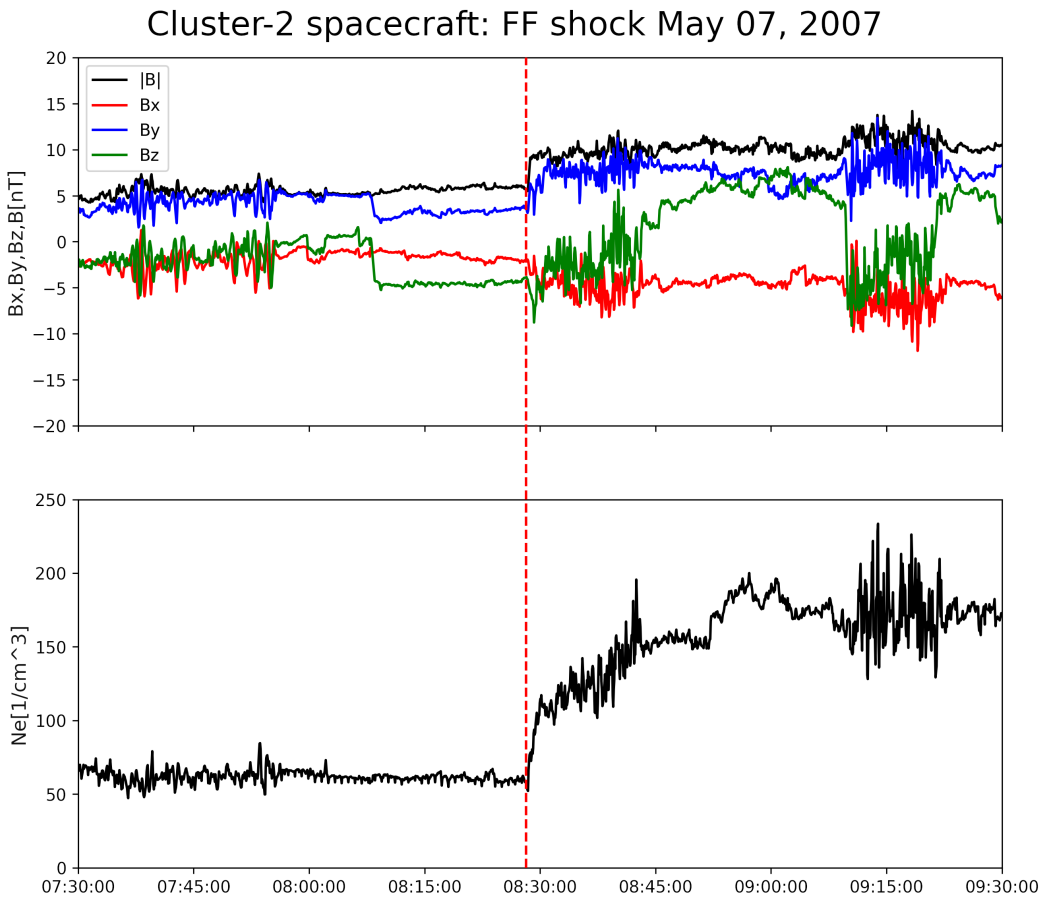


Figure 6. The plot of the shock detected by the Cluster SC2 on May 7, 2007, at 08:28:10 (UTC). The panels show from top to bottom, the magnetic field magnitude as well as its components, and the obtained electron density from the spacecraft potential. The dashed red line represents the exact shock time. The duration of the plot is two hours.

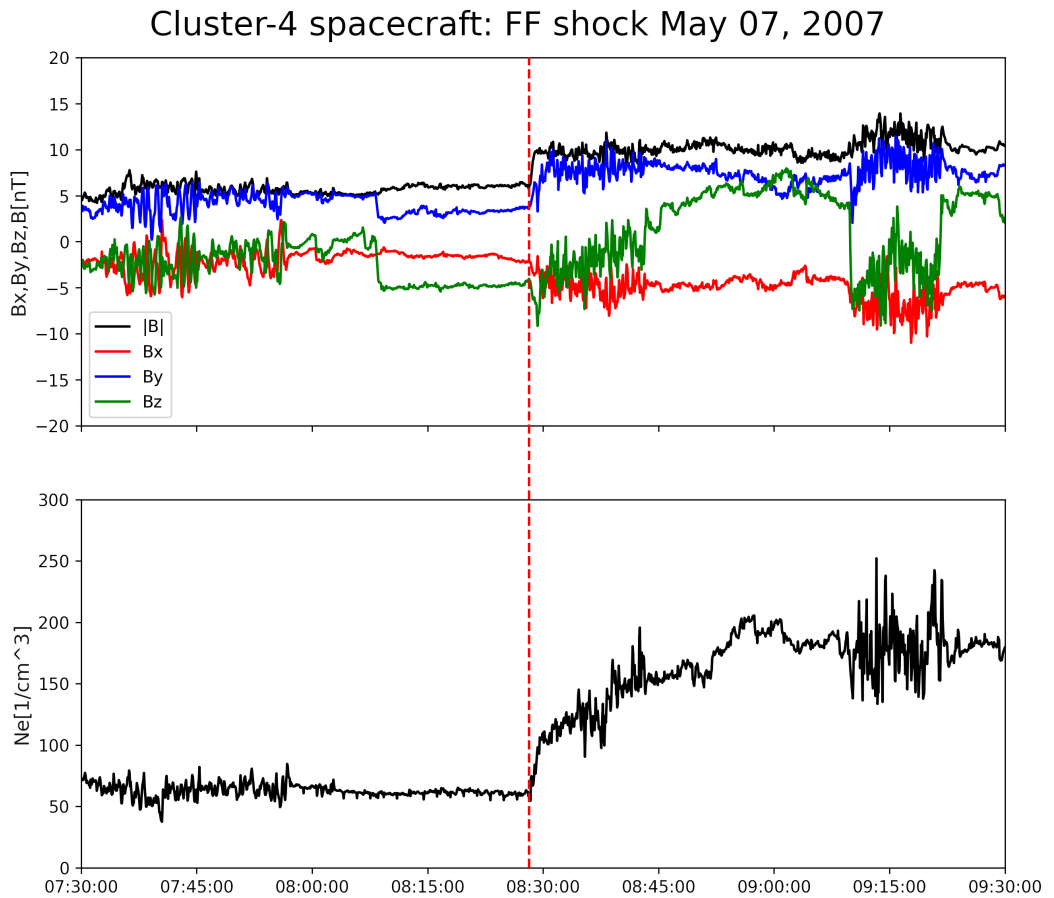


Figure 7. The plot of the shock detected by the Cluster SC4 on May 7, 2007, at 08:28:10 (UTC). The symbols and details of the figures are the same as 6. The duration of the plot is two hours.

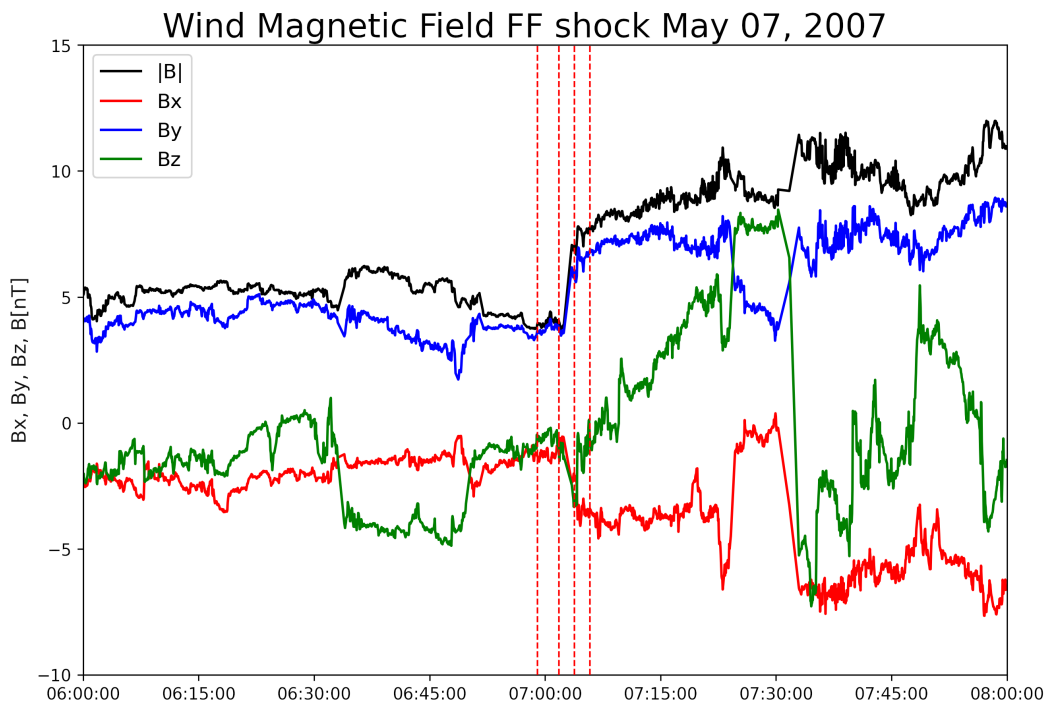


Figure 8. The Wind magnetic field measurements. The upstream Δt_{up} is between (06:59:00 - 07:01:47), and the downstream Δt_{down} is between (07:03:50 - 07:05:50). FF stands for the fast forward shock, which means the shock is traveling away from its driver. The chosen intervals of the upstream and downstream magnetic field. The red dashed lines each represent the upstream starting time and ending time and the downstream starting time and ending time, respectively

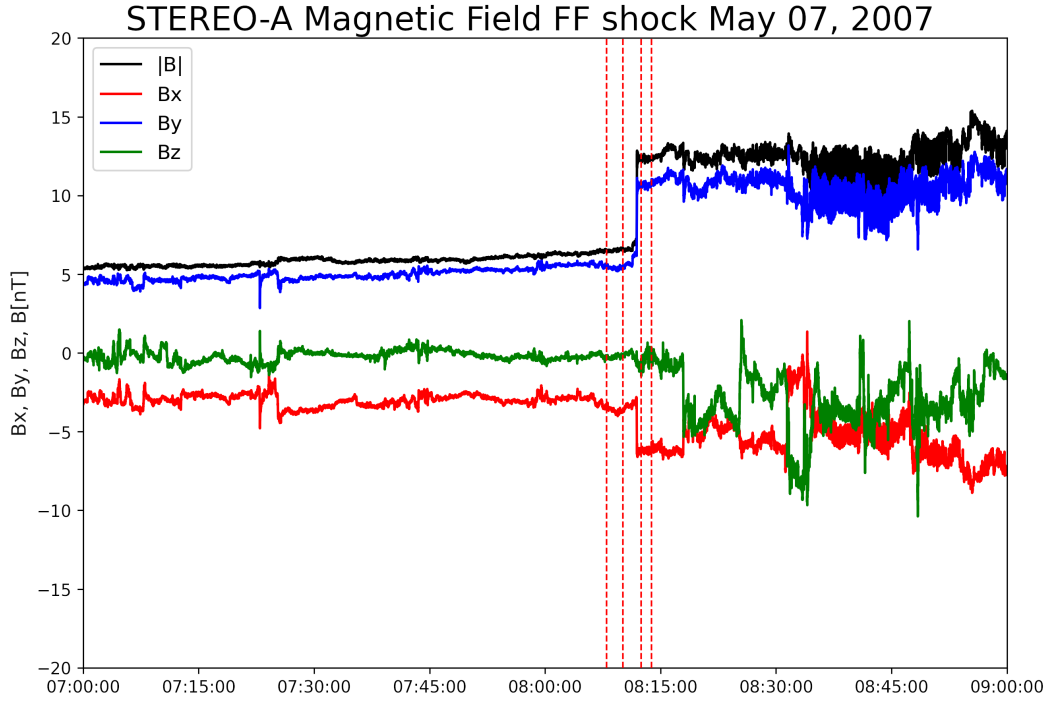


Figure 9. The STEREO–A magnetic field measurements. The upstream Δt_{up} is between (08:08:00 - 08:10:05), and the downstream Δt_{down} is between (08:12:30 - 08:13:50). The symbols and details of the figures are the same as 8

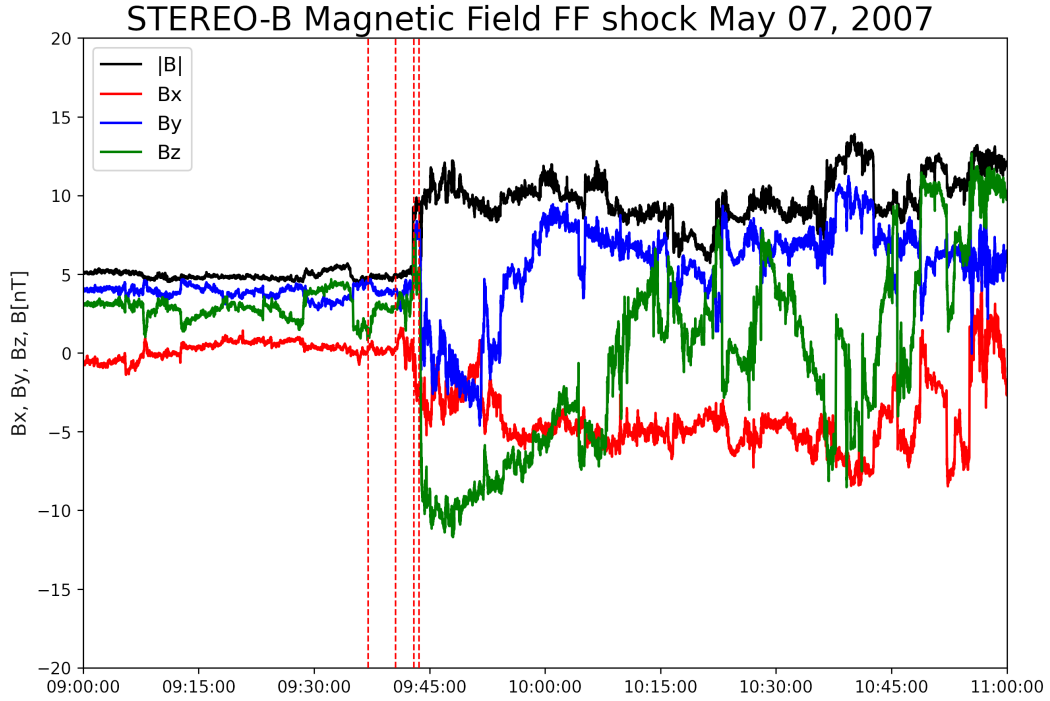


Figure 10. The STEREO–B magnetic field measurements. The upstream Δt_{up} is between (09:37:00 - 09:40:35), and the downstream Δt_{down} is between (09:42:57 - 09:43:38). The symbols and details of the figures are the same as 8

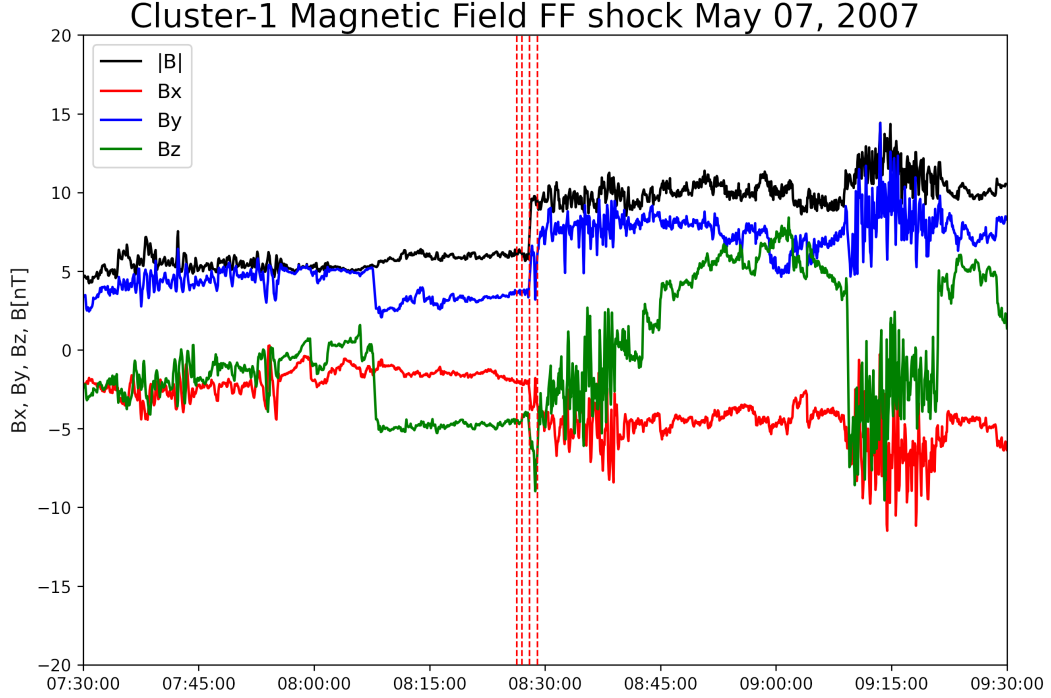


Figure 11. The Cluster-1 B magnetic field measurements. The upstream Δt_{up} is between (08:26:10 - 08:27:00), and the downstream Δt_{down} is between (08:28:00 - 08:29:00). The symbols and details of the figures are the same as 8

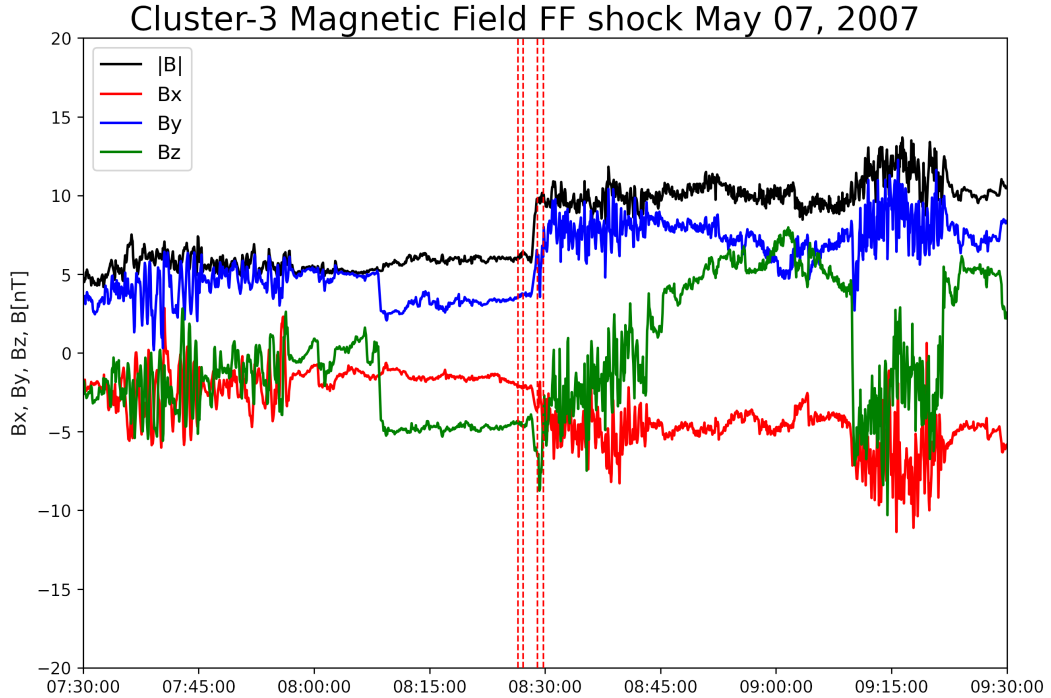


Figure 12. The Cluster-3 B magnetic field measurements. The upstream Δt_{up} is between (08:26:30 - 08:27:10), and the downstream Δt_{down} is between (08:29:00 - 08:29:47). The symbols and details of the figures are the same as 8

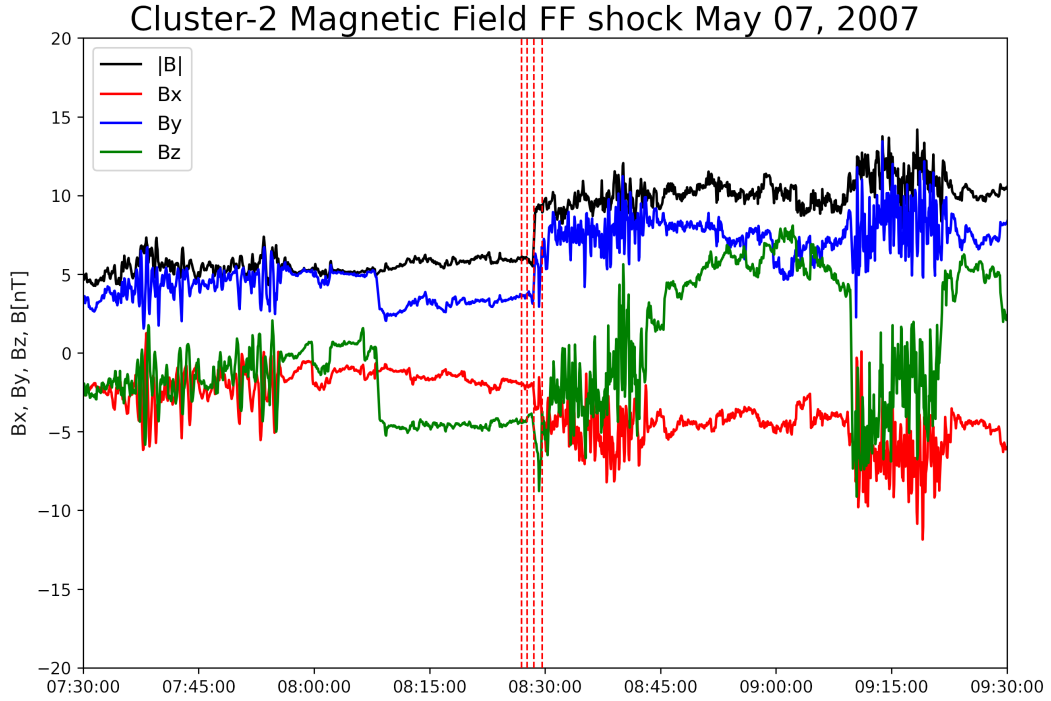


Figure 13. The Cluster-2 B magnetic field measurements. The upstream Δt_{up} is between (08:26:56 - 08:27:40), and the downstream Δt_{down} is between (08:28:32 - 08:29:37). The symbols and details of the figures are the same as 8

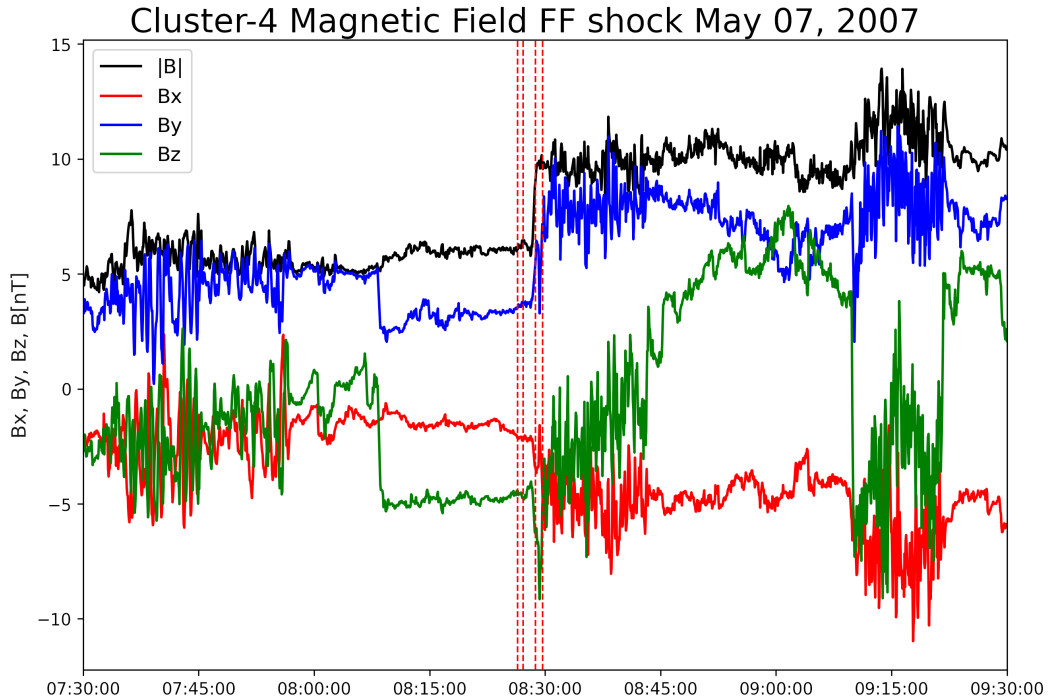


Figure 14. The Cluster-4 B magnetic field measurements. The upstream Δt_{up} is between (08:26:25 - 08:27:10), and the downstream Δt_{down} is between (08:28:45 - 08:29:40). The symbols and details of the figures are the same as 8

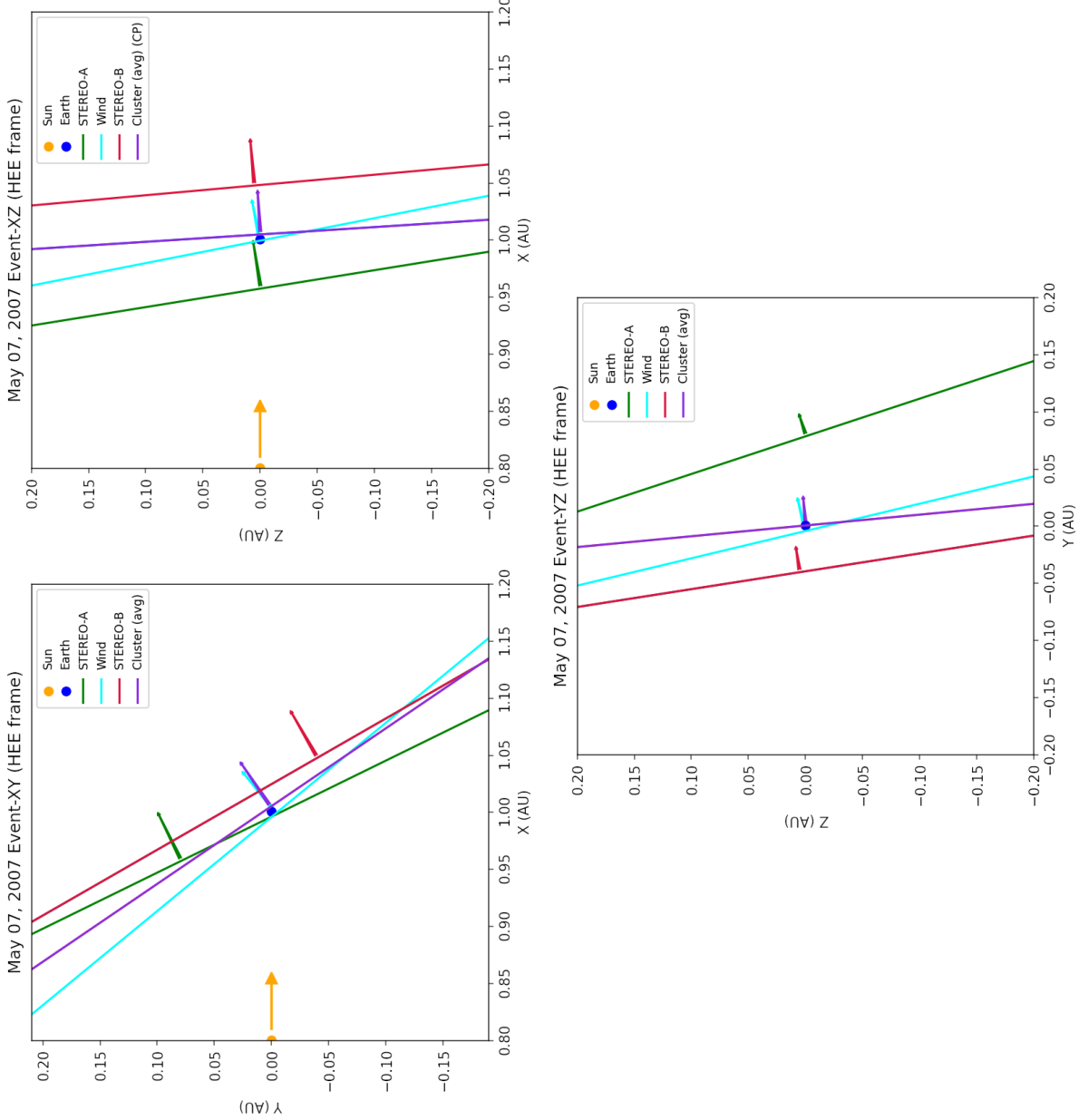


Figure 15. 2D (Top left) XY, (Top right) XZ, and (Bottom) YZ sketches of the propagation of the IP shock through spacecraft-Wind (light blue), STEREO-A (green) and B (red), and average position of four Cluster satellites (purple). The orange arrow represents the Sun-Earth line direction. The arrows on spacecraft positions indicate the normal vector direction calculated from co-planarity method and the lines perpendicular to the normal vectors indicate the shock surface orientations. The sizes of the lines are arbitrary. The shock orientations for the four Cluster satellites are averaged.

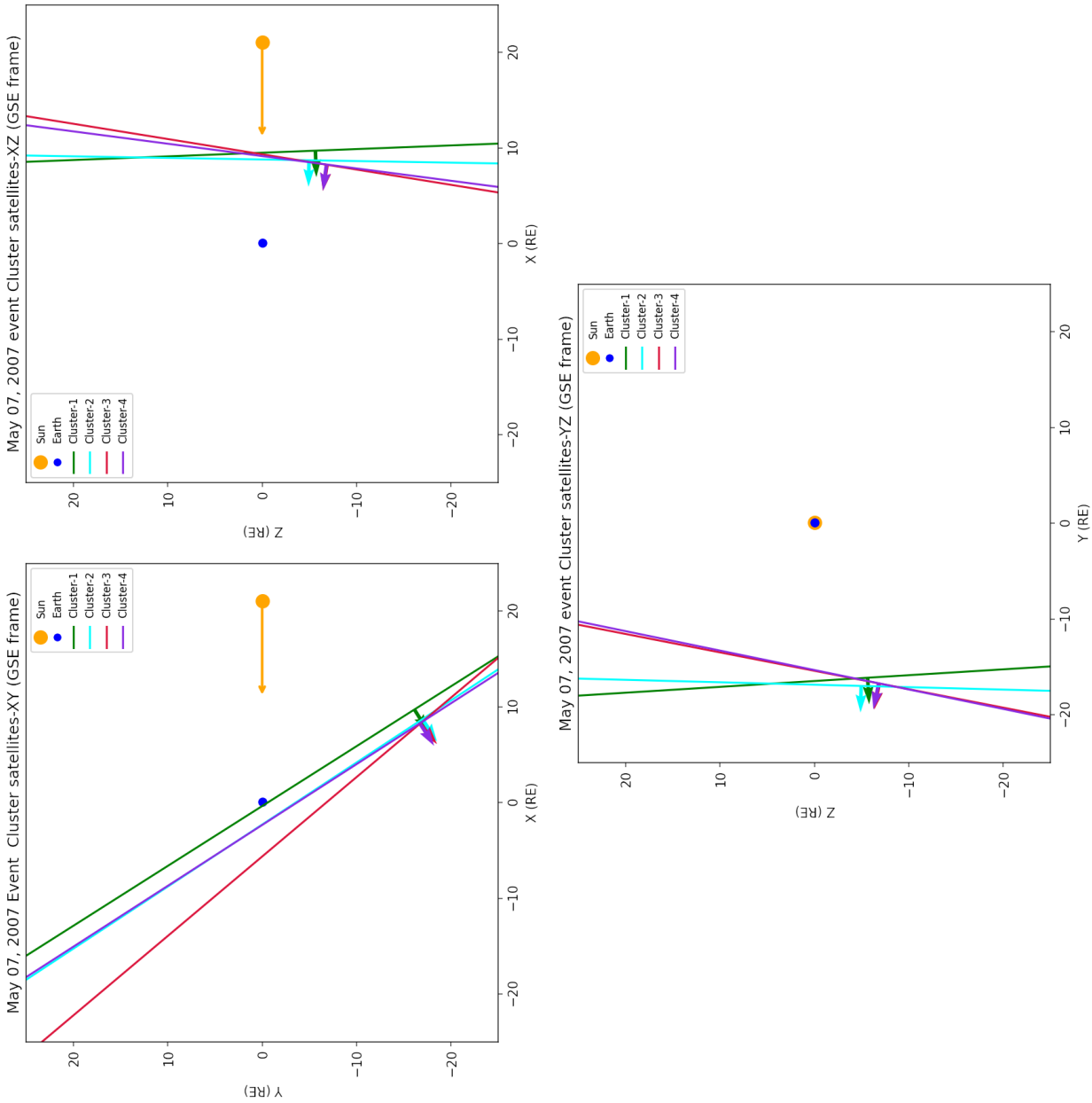


Figure 16. 2D sketch in (Top left) XY, (Top right) XZ, and (Bottom) YZ plans of the propagation of the IP shock through four Cluster satellites – SC1 (blue), SC2 (light blue), SC3 (purple), and SC4 (red). The orange arrow represents the Sun-Earth line direction. The arrows on spacecraft positions indicate the normal vector direction calculated from co-planarity and the lines perpendicular to the normal vectors indicate the shock surface orientations. The sizes of the lines are arbitrary.

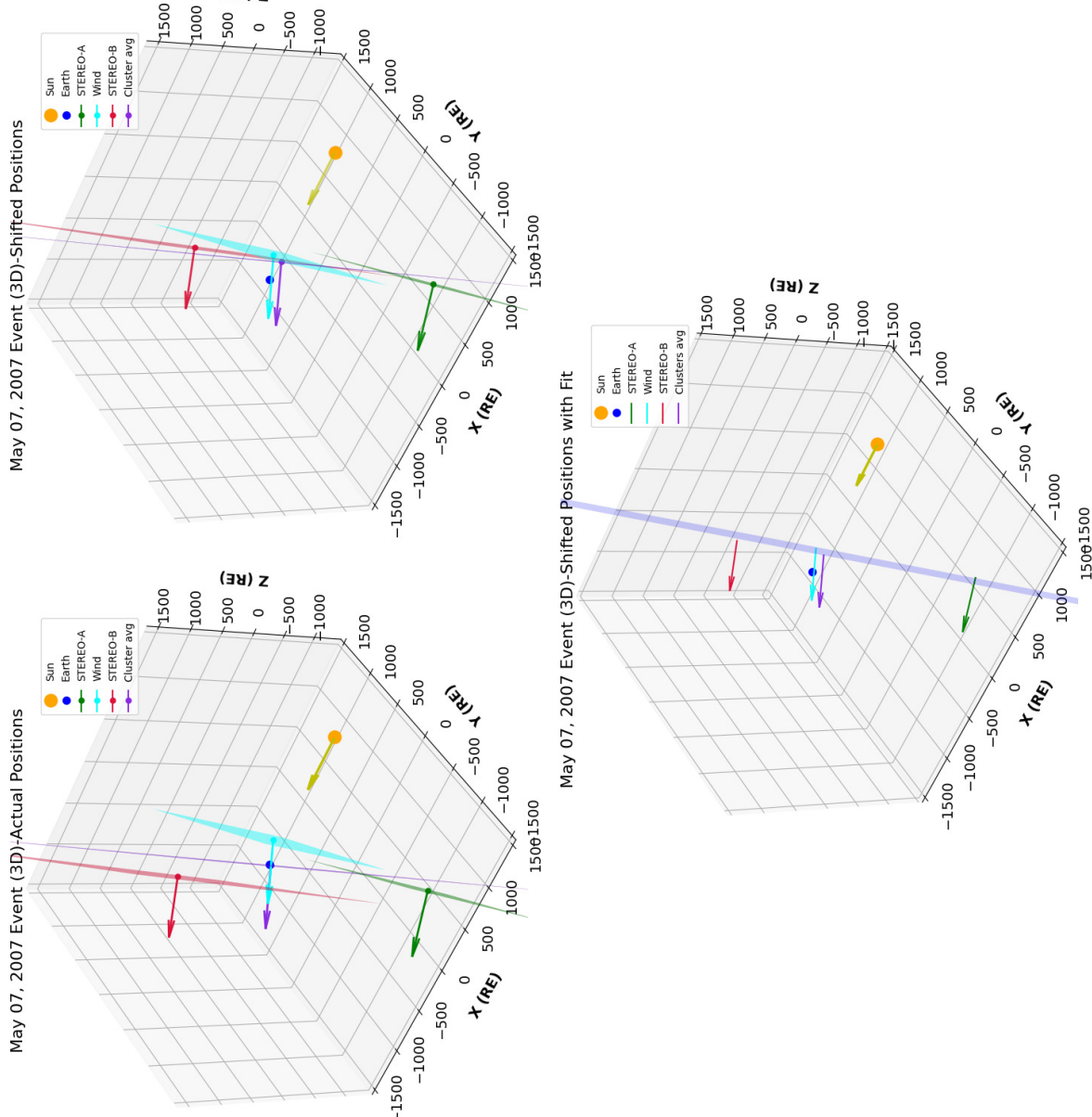


Figure 17. A 3D sketch of the propagation of the IP shock through spacecraft-Wind, STEREO-A, and STEREO-B, and average position of 4 Cluster satellites. (Top left) Actual shock detected positions. (Top right) The positions of STEREO-A, STEREO-B, and the average positions of four Cluster spacecraft are shifted back in time to the shock detection time of the Wind spacecraft. (Bottom) The time-shifted positions are fitted with a plane. The arrows indicate the normal vector direction and the planes perpendicular to the normal vectors indicate the shock surface orientations. The sizes of the planes are arbitrary.

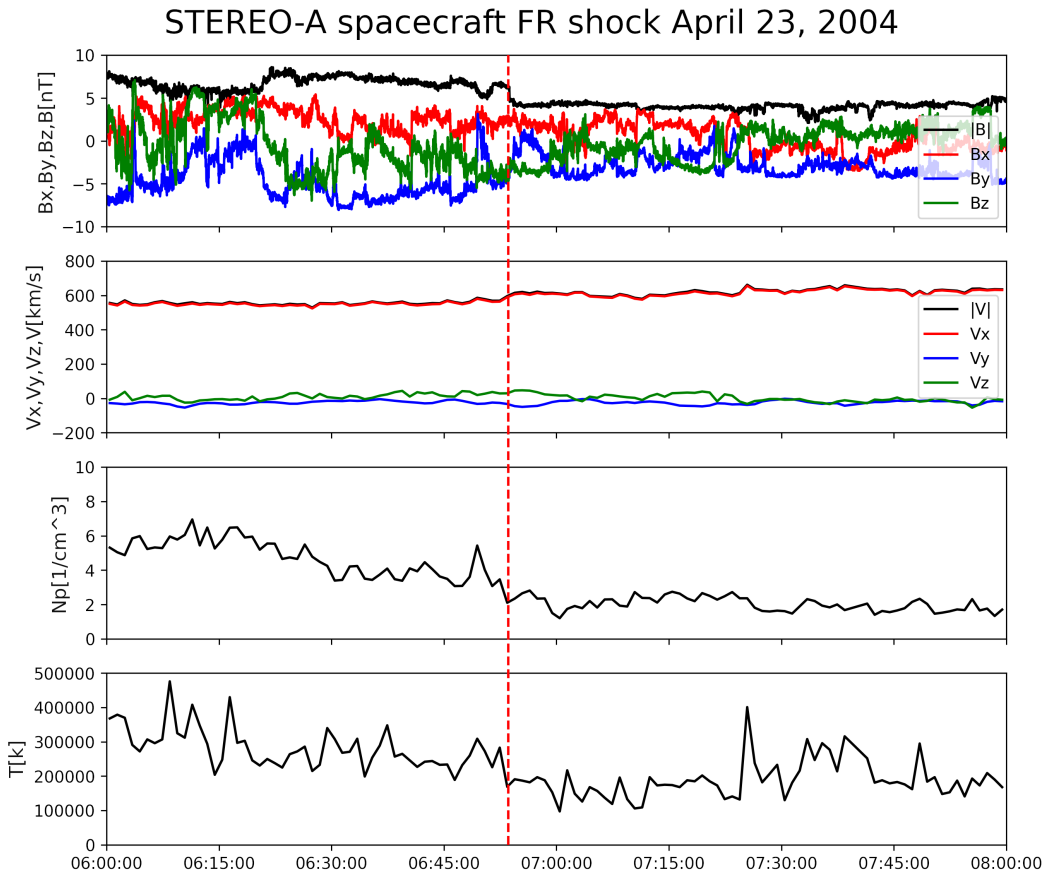


Figure 18. The plot of the shock detected by the STEREO–A spacecraft on April 23, 2007, at 06:53:35 (UTC). FR stands for the fast reverse shock, which means the shock is moving toward its driver. The panels show from top to bottom, the magnetic field magnitude as well as its components, the total velocity and its components, density, and temperature. The dashed red line represents the exact shock time. The duration of the plot is two hours

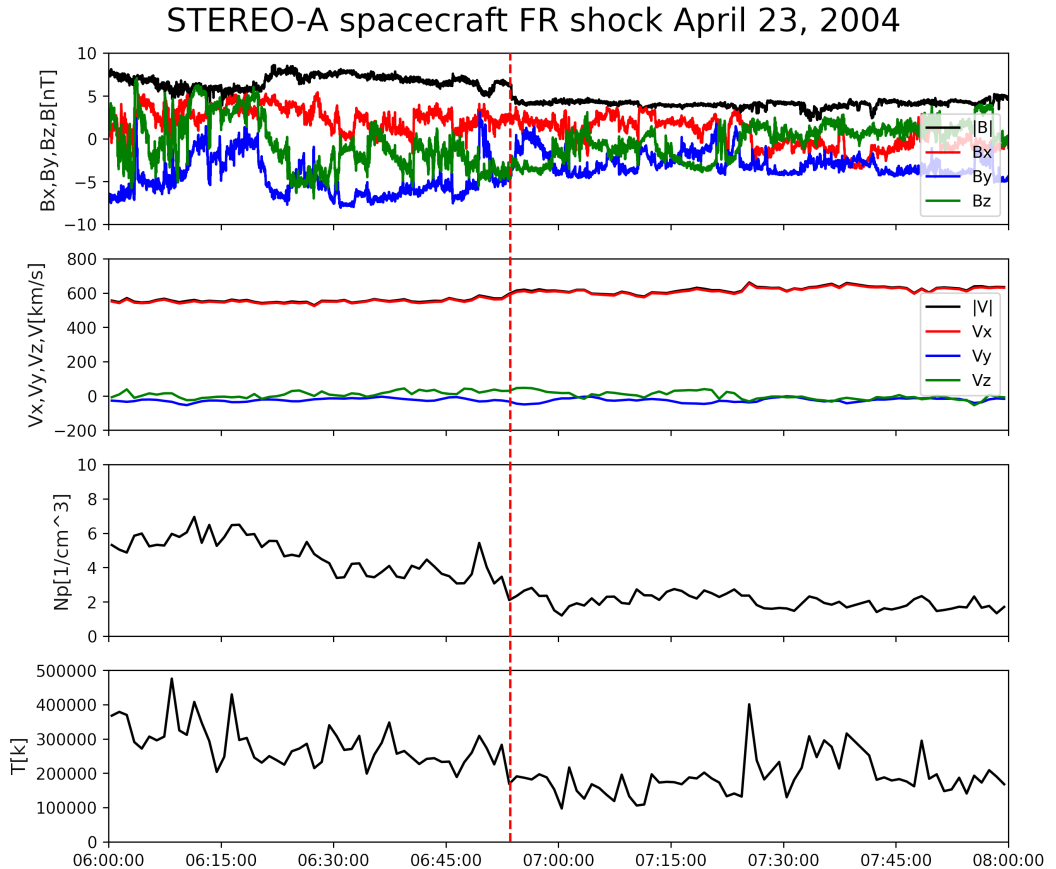


Figure 19. The plot of the shock detected by the ACE spacecraft on April 23, 2007, at 08:57:00 (UTC). The symbols and details of the figures are the same as 18. The duration of the plot is two hours.

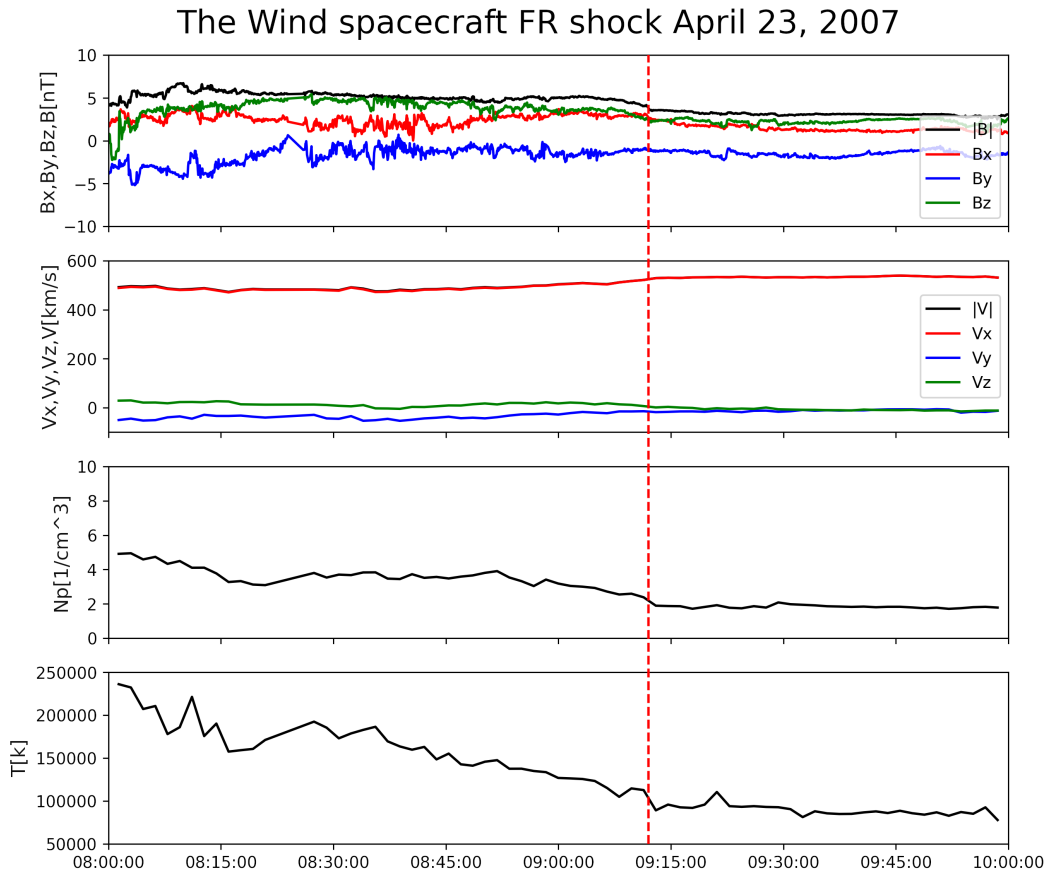


Figure 20. The plot of the shock detected by the Wind spacecraft on April 23, 2007, at 09:12:00 (UTC). The symbols and details of the figures are the same as 18. The duration of the plot is two hours.

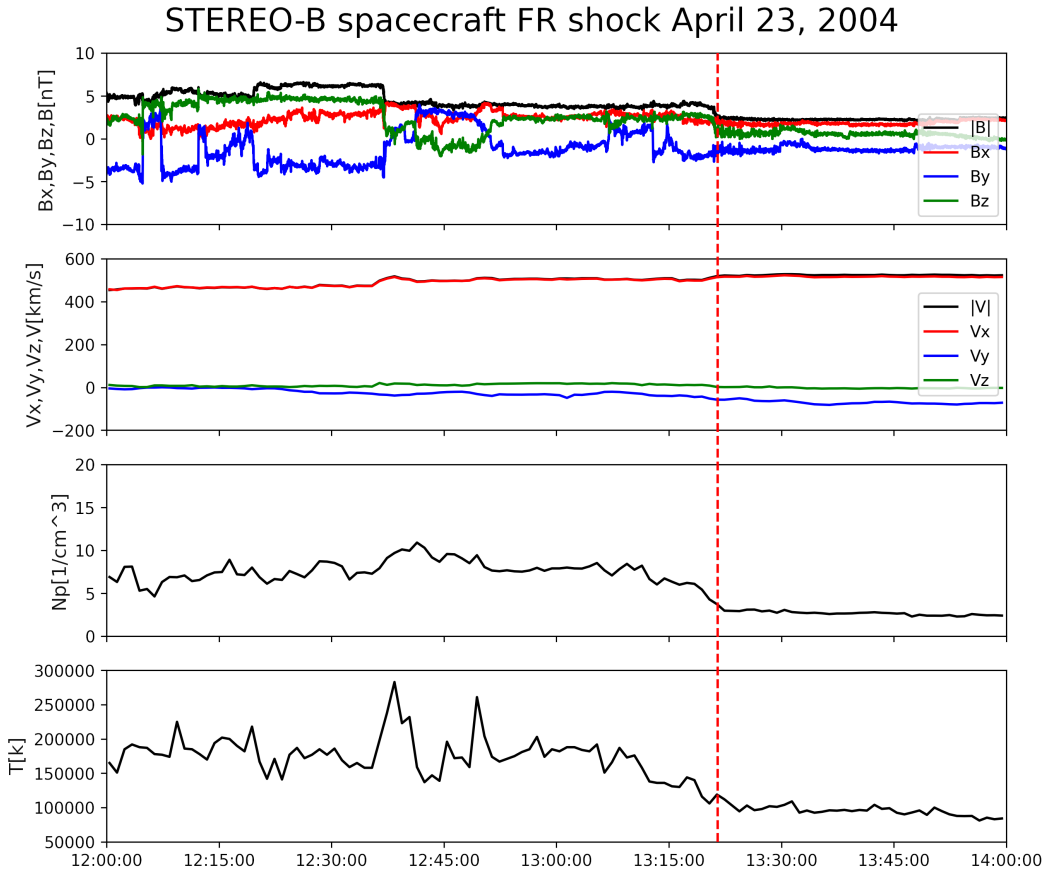


Figure 21. The plot of the shock detected by the Wind spacecraft on April 23, 2007, around 13:21:30 (UTC). The symbols and details of the figures are the same as 18. The duration of the plot is two hours.

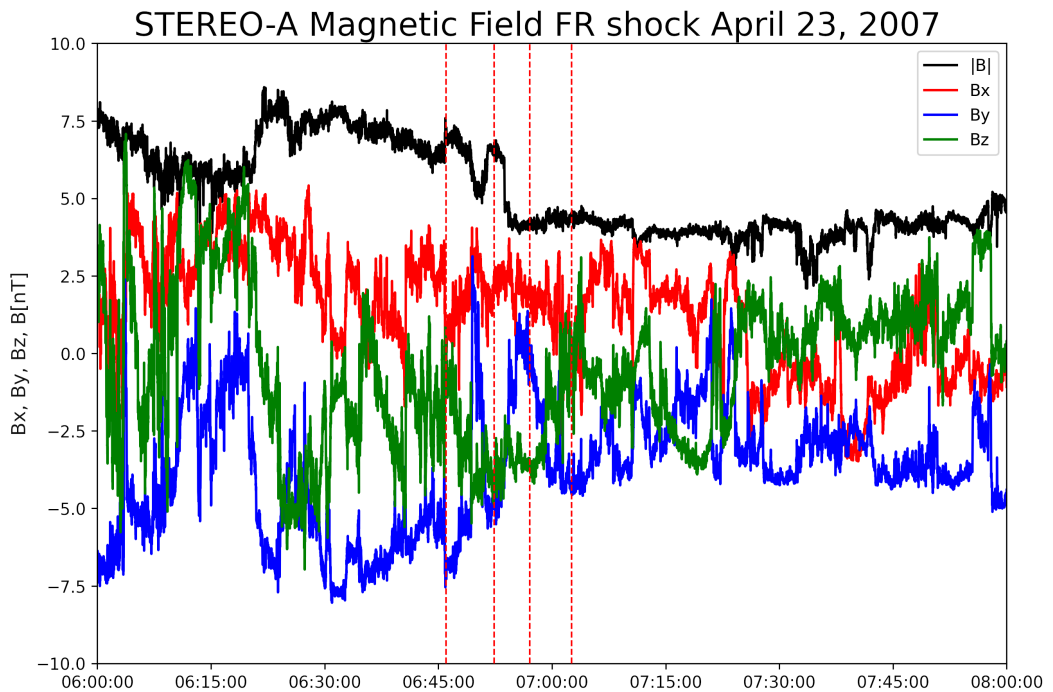


Figure 22. The STEREO–A magnetic field measurements. The downstream Δt_{down} is between (06:46:00 - 06:52:23), and the upstream Δt_{up} is between (06:57:03 - 07:02:34). FR stands for the fast reverse shock, which means the shock is moving toward its driver. The chosen intervals of the upstream and downstream magnetic field. The red dashed lines each represent the downstream starting time and ending time and the upstream starting time and ending time respectively

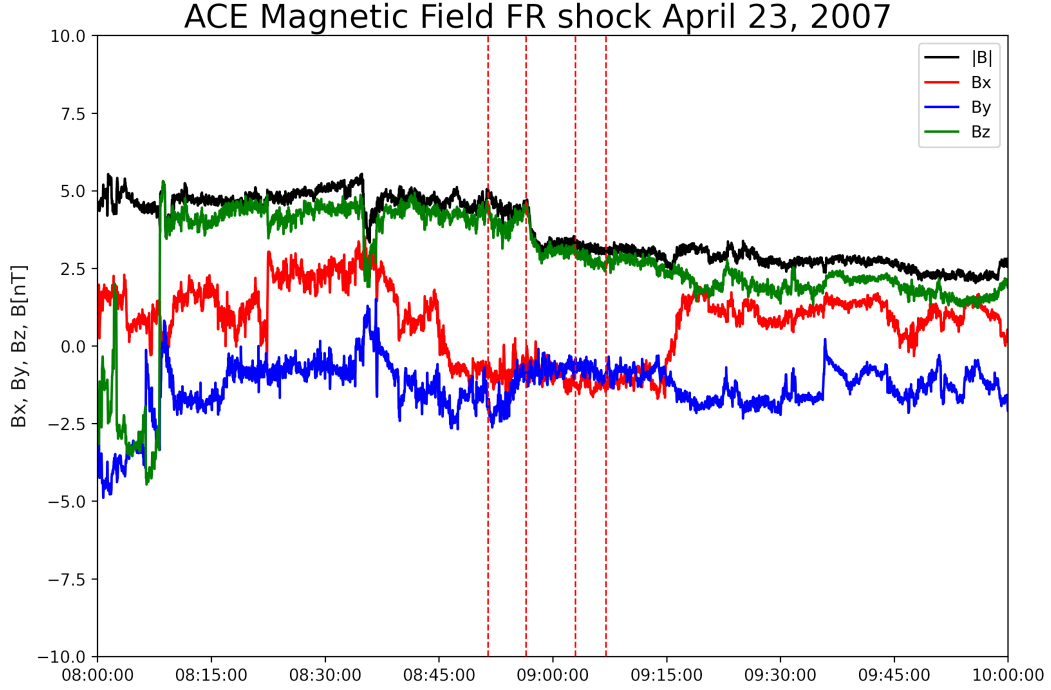


Figure 23. ACE magnetic field measurements. The downstream Δt_{down} is between (08:51:30 - 08:56:30), and the upstream Δt_{up} is between (09:03:00 - 09:07:00). The symbols and details of the figures are the same as 22

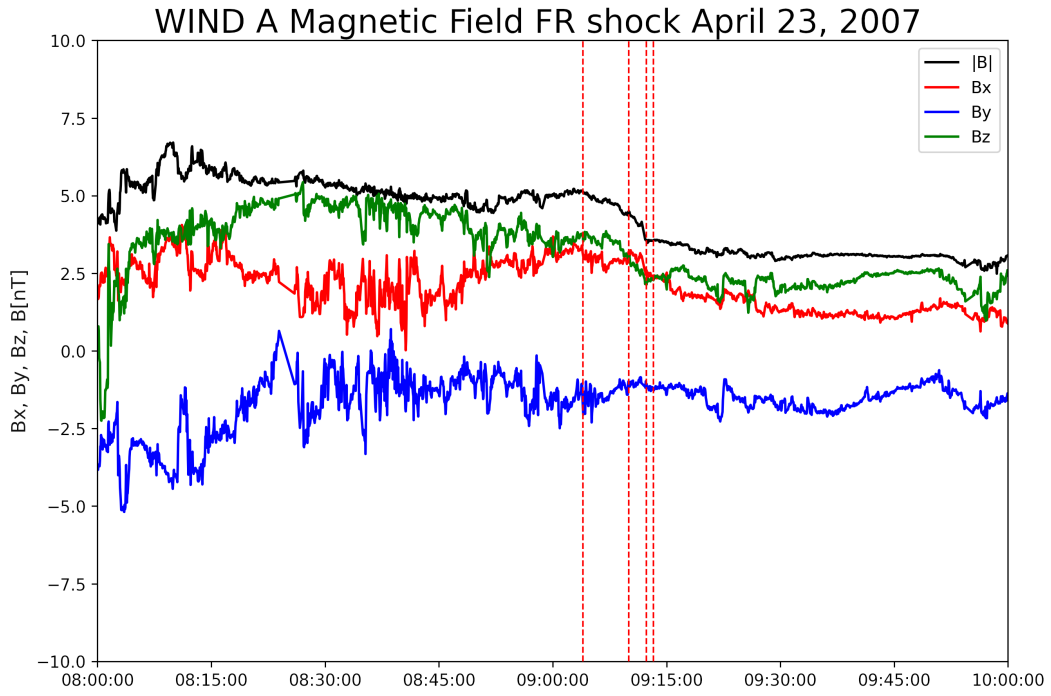


Figure 24. The Wind magnetic field measurements. The downstream Δt_{down} is between (09:04:00 - 09:10:00), and the upstream Δt_{up} is between (09:12:20 - 09:13:15). The symbols and details of the figures are the same as 22

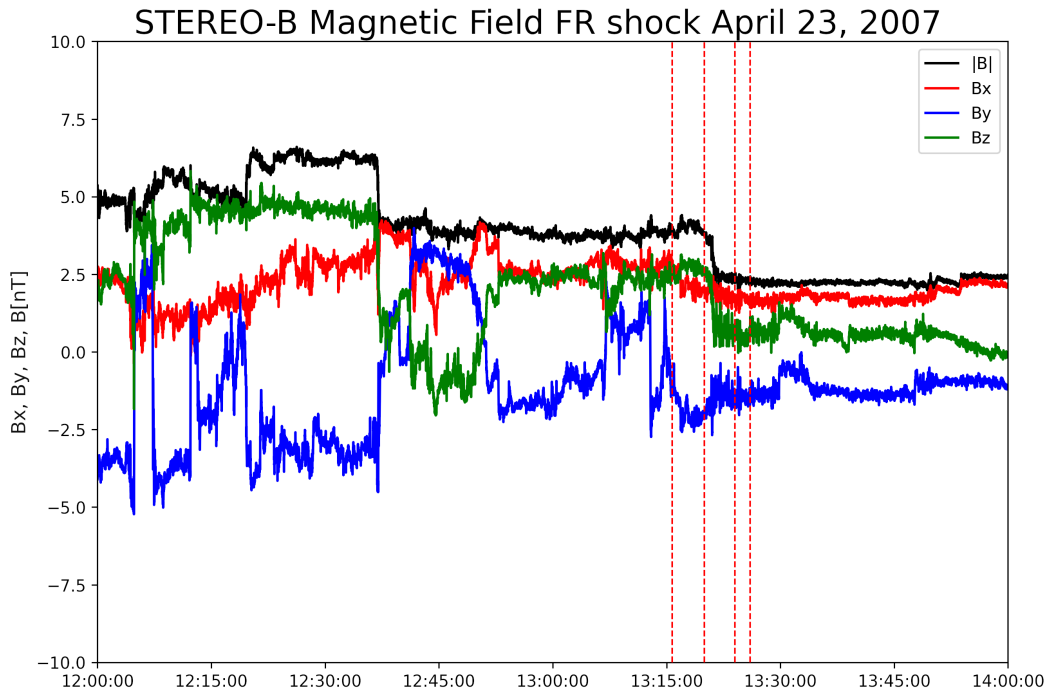


Figure 25. STEREO–B magnetic field measurements. The downstream Δt_{down} is between (13:15:45 - 13:20:00), and the upstream Δt_{up} is between (13:24:00 - 13:26:00). The symbols and details of the figures are the same as on Figure 22

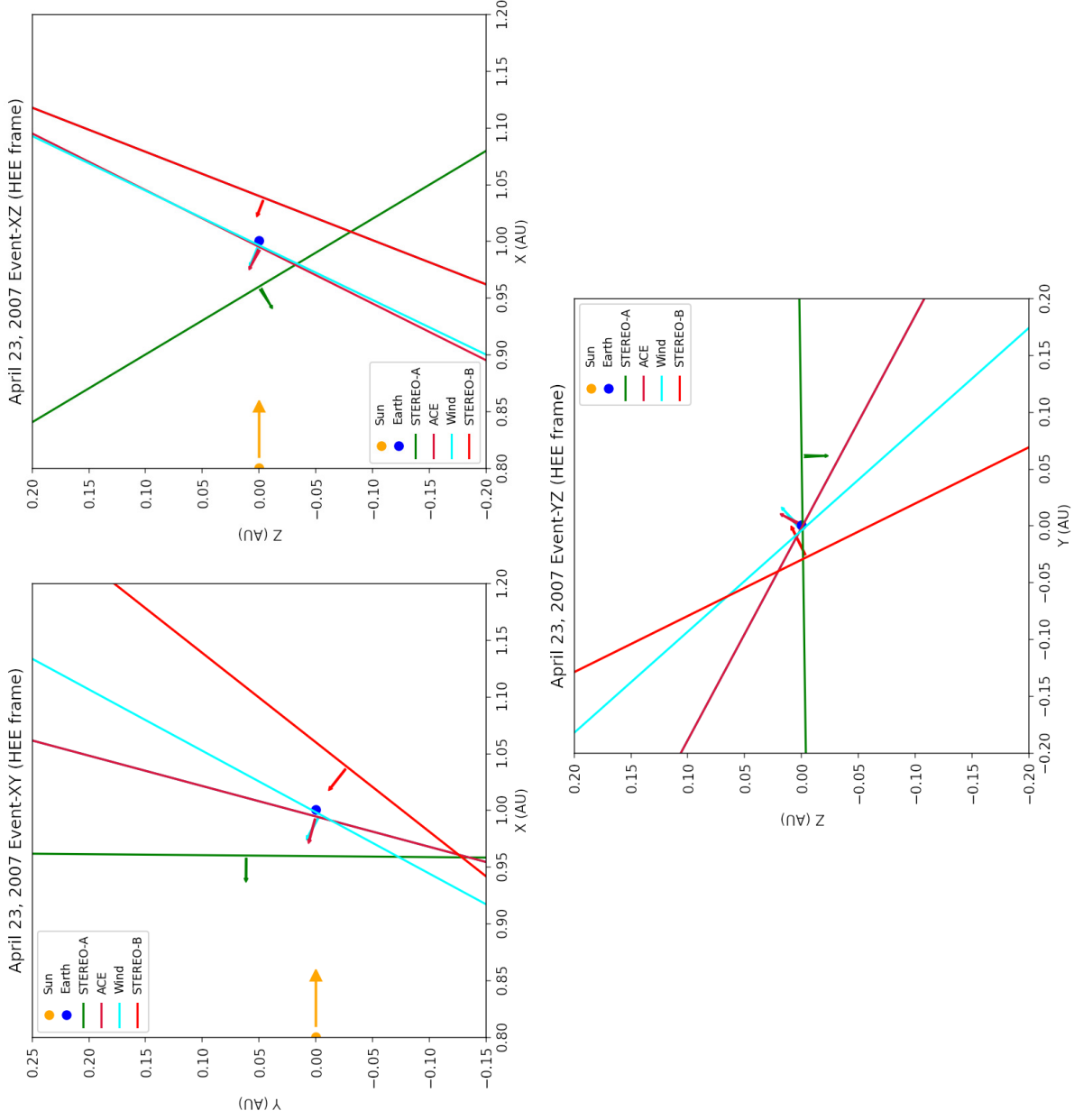


Figure 26. 2D (Top left) XY, (Top right) XZ, and (Bottom) YZ sketches of the propagation of the IP shock through spacecraft–STEREO–A, ACE, Wind, and STEREO–B. The orange arrow represents the Sun–Earth line direction. The arrows on spacecraft positions indicate the normal vector direction calculated from co-planarity method and the lines perpendicular to the shock surface orientations. The sizes of the lines are arbitrary.

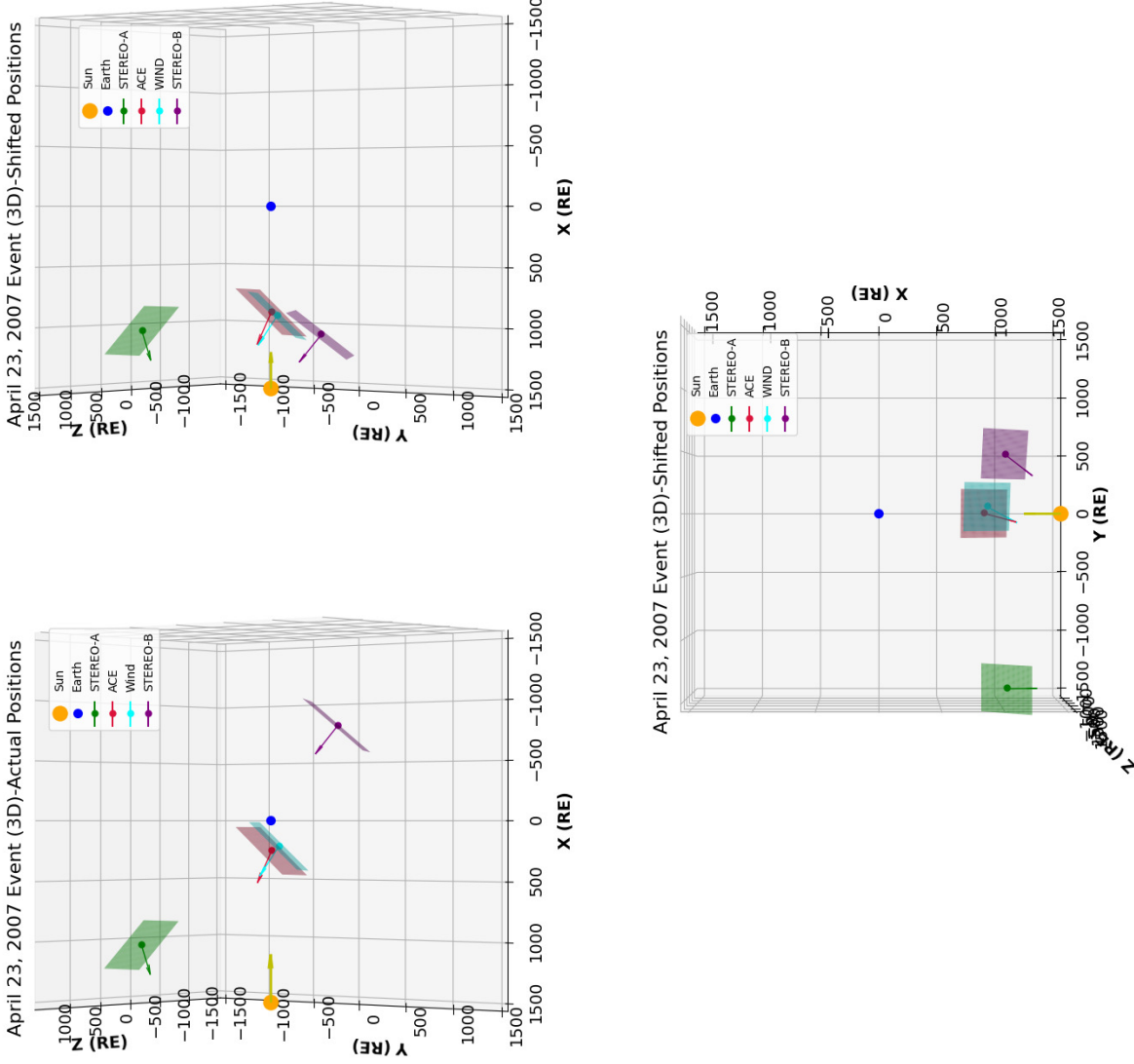


Figure 27. (Top left) A 3D sketch of the propagation of the IP shock through four spacecraft—STEREO–A, Wind, ACE, and STEREO–B. (Top right) The positions of Wind, ACE, and STEREO–B are shifted back in time to the shock detection time of STEREO–A. (Bottom) The shifted positions are shown from the top view. The arrows indicate the normal vector direction and the planes perpendicular to the normal vectors indicate the shock surface orientations. The sizes of the planes are arbitrary.

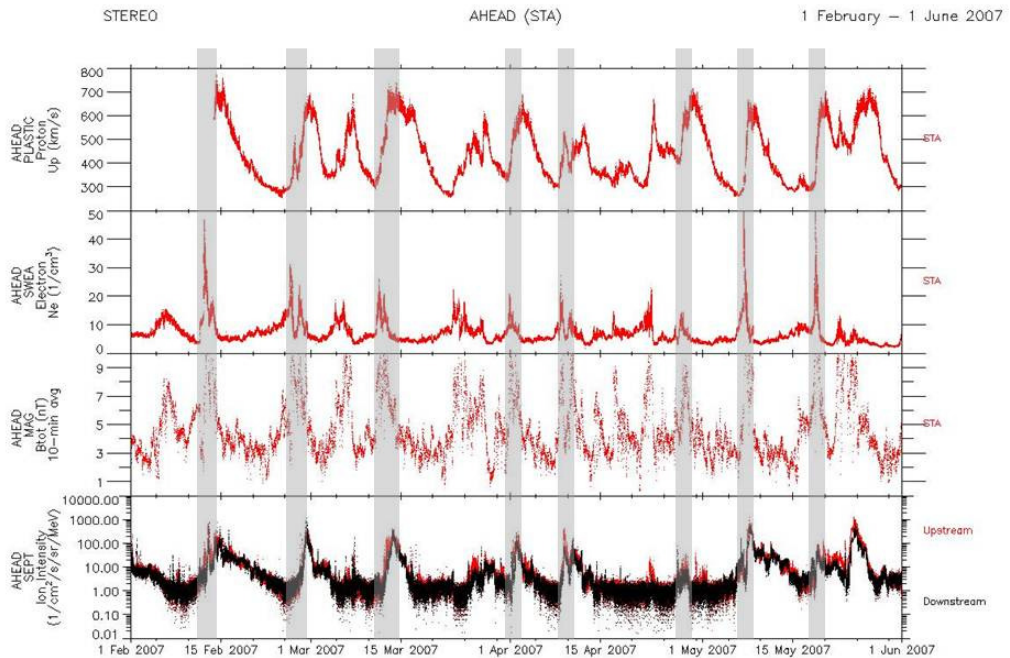


Figure 28. STEREO–A PLASTIC bulk velocity, the SWEA electron density, MAG magnetic field magnitude, and the SEPT ion intensity from 110 keV to 2200 keV. Periods featuring well-established Co-rotating Interaction Regions (CIRs) from February 1, 2007 to June 1, 2007. It illustrates theeable boosts in ion energy are highlighted with grey shading (Opitz et al., 2014, Figure 2).

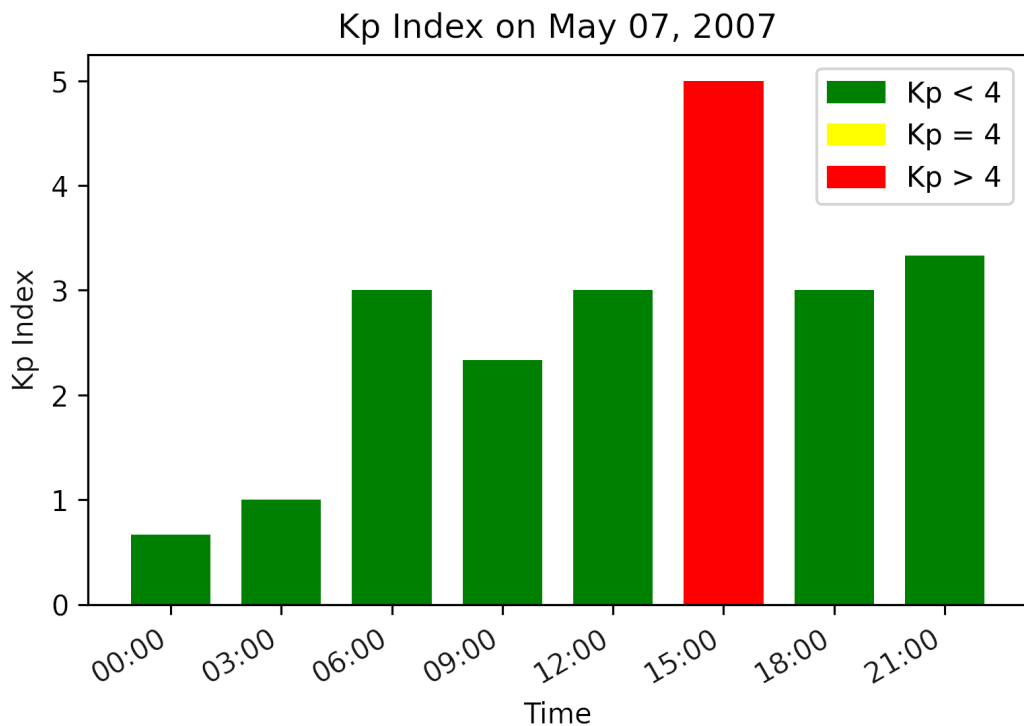


Figure 29. K_p -index on May 07, 2007. The green bar indicates moderate geomagnetic activity, while the yellow bar denotes intensifying geomagnetic activity with the red bar being a geomagnetic storm. Here, the red bar indicates a G1-minor geomagnetic storm.

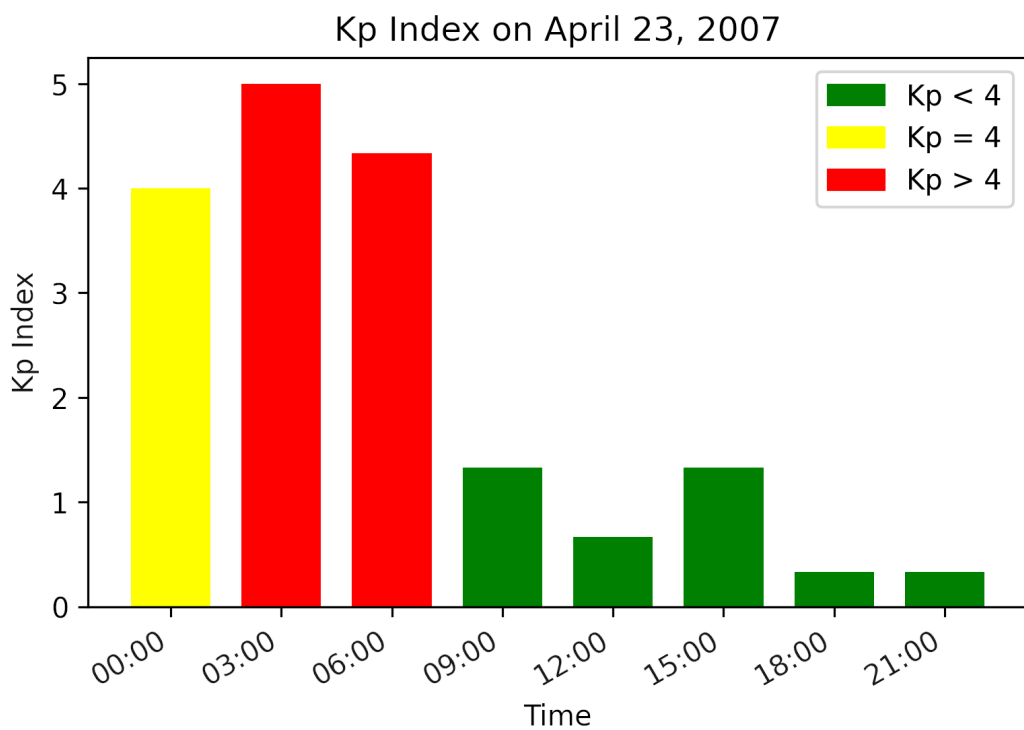


Figure 30. The K_p -index on April 23, 2007. The symbols and details of the figure is the same as on Figure 29